

DEVELOPMENT OF A NONINVASIVE OPTICAL AND THERMOGRAPHIC IMAGING
PROTOCOL FOR IDENTIFICATION OF PEDIATRIC LOW CARDIAC OUTPUT
SYNDROME

By

Rachel Clare Ping

Thesis

Submitted to the Faculty of the
Graduate School of Vanderbilt University
in partial fulfillment of the requirements
for the degree of

MASTER OF SCIENCE

in

Biomedical Engineering

December 18th, 2021

Nashville, TN

Approved:

Dr. Justin Baba, PhD

Dr. Cynthia B. Paschal, PhD

TABLE OF CONTENTS

ACKNOWLEDGEMENTS	iv
LIST OF TABLES	vi
LIST OF FIGURES	vii
Chapter:	
I. INTRODUCTION AND LITERATURE REVIEW	1
1.1 Congenital Heart Disease	1
1.2 Low Cardiac Output Syndrome	3
<i>1.2.1 Motivation</i>	<i>3</i>
<i>1.2.2 Clinical Presentation and Diagnosis</i>	<i>3</i>
<i>1.2.3 Etiology of LCOS</i>	<i>8</i>
<i>1.2.4 Risk Factors for LCOS.....</i>	<i>9</i>
<i>1.2.5 Postoperative Management of LCOS.....</i>	<i>10</i>
<i>1.2.6 Hemodynamic Monitoring</i>	<i>11</i>
<i>1.2.7 Core-Peripheral Temperature Gradients</i>	<i>12</i>
1.3 Medical Thermography.....	17
1.4 Objectives and Aims	19
II. THERMOGRAPHIC QUANTIFICATION PROTOCOL.....	20
2.1 Clinical Study Deployment.....	20
2.2 Processing Software	25
2.3 Software Procedure.....	26
<i>2.3.1 Vital Data Entry</i>	<i>27</i>
<i>2.3.2 Image Conversion</i>	<i>29</i>
<i>2.3.3 Image Quality.....</i>	<i>30</i>
<i>2.3.4 Image Registration and Segmentation</i>	<i>33</i>
<i>2.3.5 Post Analysis Processing Methods</i>	<i>39</i>

III. CASE ANALYSIS AND DISCUSSION	40
3.1 Pilot Study Analysis	40
3.1.1 <i>Case 1: Background</i>	40
3.1.2 <i>Discussion</i>	41
3.2 Pilot Study Analysis	45
3.2.1 <i>Case 2: Background</i>	45
3.2.2 <i>Discussion</i>	46
IV. CONCLUSIONS AND FUTURE WORK	55
1.1 Conclusions	55
2.1 Future Work	55
REFERENCES	59
APPENDICES	64
Appendix A: IRB Approved Clinical Protocol	64
Appendix B: ICI Camera Technical Specifications	73
Appendix C: Clinical Nurse Protocol	74

ACKNOWLEDGEMENTS

First, I would like to thank Dr. Justin Baba and the Vanderbilt Biophotonics Center for providing me the opportunity to learn and grow my research skills in a supportive and encouraging environment. I would also like to recognize Dr. Baba for his steadfast faith in my work and his efforts to foster my success. Without his oversight, this work would not be possible. I would also like to thank the Vanderbilt Monroe Carrell Jr. Children's Hospital, and in particular, Dr. Isaura Diaz, MD, and Dr. Neil Zaki, MD for their extensive collaboration throughout this study. Their extensive contributions and commitment towards elevating the standard of pediatric cardiac care reflects their core values as extraordinary physicians. I would also like to recognize Dr. Cynthia Reinhart-King and the Biomedical Engineering Department at Vanderbilt for the opportunity to study at a world-class university and to learn from the most caring and committed instructors, researchers, and mentors.

Secondly, I would like to acknowledge and thank my family for their love and care throughout the pursuit of my degree. I would like to thank my eldest sister, Ally, and her husband, Alex, for housing me and providing me with every ounce of support that they could provide throughout my time in Nashville. They provided me not only with a room, but a home and space to where I could flourish in graduate school; their companionship and friendship have been a constant source of inspiration. I would also like to thank my middle sister, Michaela, for her joy and uplifting kindness that have helped carry me through the difficult times. Your bright spirit has brought me happiness and laughter on my darkest days and reflects your endlessly caring and generous heart.

Lastly, I would like to thank my partner, Joshua, for never failing to believe in me and being my rock throughout my college years. Despite any distance, and despite any difficulties, you have always stood by my side and never wavered in the face of challenges. There are never enough words to capture all of your incredible character and qualities, but I hope that you know that I am in continuous awe of your good-natured spirit, compassion, and loyalty to your family and friends. Thank you for your friendship, your partnership, and your love throughout the years. I can never thank you enough for how much you have sacrificed for me and for the sheer joy that you bring to my life. I love you! I would also like to recognize your family, who have welcomed me with open arms and given me so much love and encouragement. It is truly extraordinary to see the community

you all have fostered, and it is certainly because of your generosity and kindness that people look to you for companionship.

Finally, I would like to thank my lifelong friends and teammates along the way who have always taught me so many life lessons and filled my life with joy. Maddie and Nicole, thank you for being my soul sisters and giving me a lifetime of happy memories, love and support.

LIST OF TABLES

Table 1: Software Specifications	25
Table 2: List of Recorded Vital Values	27
Table 3: Observed and Calculated Hemodynamic Monitoring Values (Case 1)	41
Table 4: Observed and Calculated Hemodynamic Monitoring Values (Case 2)	46
Table 5: Hemodynamic Values Comparison at $T = 3H$ (Case 2)	47
Table 6: Normal Reference Hemodynamic Values for Infants.....	48

LIST OF FIGURES

Fig. 1: Birth Prevalence of CHD Subtypes	2
Fig. 2: Correlation between cardiac index and toe temperature.....	14
Fig. 3: Coupled Imaging System Mount.....	22
Fig. 4: Clinical Deployment of Coupled Imaging System.....	23
Fig. 5: Alternative Views- Clinical Deployment of Coupled Imaging System	23
Fig. 6: Software Protocol Illustration.....	26
Fig. 7: Example Vital Sheet and Excel Entry	28
Fig. 8: Editing Temperature Axes.....	29
Fig. 9: 6 Regions of Interest (ROIs).....	30
Fig. 10: Comparison Between "Good" and "Bad" Images.....	31
Fig. 11: Image Quality Application Steps.....	32
Fig. 12: Image Registration Control Points- Head.....	34
Fig. 13: Image Registration Control Points- Body.....	34
Fig. 14: ROI Screening Query	36
Fig. 15: Example ROI Selection	36
Fig. 16: Typical Thermographic Report Card.....	37
Fig. 17: Incomplete Thermographic Report Card.....	38
Fig. 18: Mean Cardiac Output over Time (Case 1).....	42
Fig. 19: Mean Core Chest Temperature over Time (Case 1).....	43
Fig. 20: Core Peripheral Foot Temperature Gradient over Time (Case 1)	44
Fig. 21: Cardiac Output (L/min) over Time (Case 2)	49
Fig. 22: Systolic Blood Pressure over Time (Case 2)	50
Fig. 23: Mean Core Chest Temperature over Time (Case 2).....	50
Fig. 24: Peripheral Hand Temperature Over Time (Case 1).....	51

Fig. 25: Peripheral Hand Temperature Over Time (Case 2)..... 52

Fig. 26: Core-Peripheral Hand Temperature Gradient Over Time (Case 1)..... 53

Fig. 27: Core-Peripheral Hand Temperature Gradient over Time (Case 2)..... 54

Fig. 28: Cycle Tracker Report Card..... 57

LIST OF ABBREVIATIONS

AI	Artificial Intelligence
ART	Arterial Pressure
ASD	Atrial Septal Defect
BPM	Beats Per Minute
cAMP	Cyclic adenosine monophosphate
CBC	Complete Blood Count
CHD	Congenital Heart Defect
CI	Cardiac Index
CO	Cardiac Output
CPB	Cardiopulmonary Bypass
CPTG	Core-Peripheral Temperature Gradient
CVP _m	Central Venous Pressure
DBP	Diastolic Blood Pressure
DSC	Delayed Sternal Closure
EHR	Electronic Health Record
FPS	Frames Per Second
HR	Heart Rate
IR	Infrared
IRB	Institutional Review Board
IRI	Ischemic Reperfusion Injury
LCOS	Low Cardiac Output Syndrome
MAP	Mean Arterial Pressure
NIRS	Near-Infrared Spectroscopy
NO	Nitric Oxide
PDA	Patent Ductus Arteriosus
Perf	Perfusion
PI	Principal Investigator
PICU	Pediatric Intensive Care Unit

PVC	Premature Ventricular Contractions
ROI	Region of Interest
RR	Respiration Rate
SBP	Systolic Blood Pressure
ScVO ₂	Central Venous Oxygen Saturation
SpO ₂	Oxygen Saturation
SvO ₂	Venous Oxygen Saturation
SV	Stroke Volume
SVR	Systemic Vascular Resistance
VIS	Visual
VSD	Ventricular Septal Defect

CHAPTER I

INTRODUCTION AND LITERATURE REVIEW

1.1 Congenital Heart Disease

Congenital heart disease (CHD) is an umbrella term that collectively describes a variety of conditions affecting normal development of the heart yielding irregular hemodynamic patterns in neonates and newborns. While there are a few forms of CHD that do not pose an imminent risk to a newborn, most complicate a child's development and can lead to serious, life-threatening conditions if left untreated. Generally, CHD is diagnoseable during the second or third trimester of pregnancy using fetal echocardiograms; however, a decreased size and/or challenging in utero imaging environment can make it difficult to diagnose, [1, 2]. The current standard of care for the most critical CHD patients is early surgical intervention (<6 months of age), followed by hospitalization in a pediatric intensive cardiac care unit, and/or extended management of symptoms with medication. While only a quarter of those diagnosed with CHD may require immediate surgical intervention, the lifelong ramifications of CHD on quality of life and overall health cannot be understated [3]. Individuals who survive childhood with CHD have a reduced lifespan compared to their peers, are more likely to have developmental complications, and are more likely to experience serious conditions: such as heart failure. Though advancements in pediatric and neonatal surgeries have helped reduce mortality for this fragile population, there are still numerous complications and uncertainties associated with the treatment of CHD [4].

CHD is a growing concern in the medical community, as it has become the most common birth defect globally. The prevalence is significant, as CHD is diagnosed in 8 children per 1,000 live births, or 1 in 100 births [3]. The distribution of diagnosis is independent of several factors, including geographical location and average national income, indicating that the disease is a global challenge and that its resolution is immensely beneficial worldwide. Recent analysis of the literature suggests that the burden of this disease has continued to increase after a brief period of stabilization between the years 2000 and 2017 [2,3,5]. While the noted increase of diagnoses may be partially attributed to improved imaging and diagnostic methods, it does not minimize the need for addressing CHD. Rather, it highlights the importance of resolving or managing it as the overall number of patients living with CHD complications has increased.

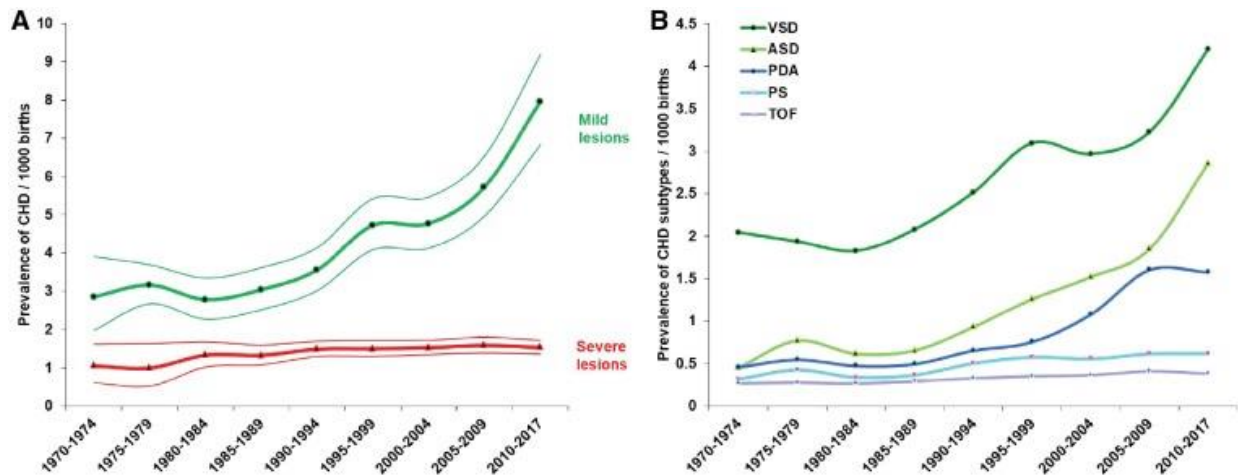


Fig. 1: Birth Prevalence of CHD Subtypes. The birth prevalence of CHD subtypes and their changes over time. (A) The prevalence of mild and severe CHD lesions during 1970–2017. Thick lines are the estimated prevalence of CHD lesions, thin lines represent the 95% CI. (B) The birth prevalence of the five most frequent CHD subtypes during 1970–2017. VSD, ventricular septal defects; ASD, atrial septal defects; PDA, patent ductus arteriosus; PS, pulmonary stenosis; TOF, tetralogy of Fallot. Adopted from Ref. [2]

Though congenital heart disease can present itself in various forms of defects and in their combinations, milder lesions are the most reported form of CHD at birth. Three types of defects comprise the most common lesions reported at birth globally: ventricular septal defects (VSD), atrial septal defects (ASD), and patent ductus arteriosus (PDA). Since 1970, the reported rates of these mild lesions have increased almost threefold. Therefore, treatment of these conditions is relevant and important when studying CHD in neonates and infants (Fig. 1). Advancements in imaging and diagnostic procedures have greatly reduced early mortality in this population, and over ninety percent of individuals diagnosed with CHD are expected to survive through adulthood with modern treatment. However, outcomes from surgical interventions have failed to measure up to improved diagnosis rates, as the overall mortality rate for all defect repairs has stabilized at thirteen percent over the same period of analysis [4].

While advanced CHD surgical techniques, informed preoperative planning, and improved imaging techniques have helped reduce major causes of mortality during operative procedures, they have not necessarily improved overall mortality. In particular, the postoperative recovery stage is still a complicated and widespread challenge to physicians, as significant morbidity and mortality is attributed to this period. This is especially concerning when considering the distribution of surgical cases by population. In fact, the number of neonates and infants requiring surgery increased from 26% to just over 40% in the early 2000s alone. Surgical outcomes in this population carry an early mortality rate of 10% in a significantly large and growing population that requires invasive treatment [6]. Since its inception in the 1950s, cardiopulmonary bypass (CPB) has been a greatly utilized surgical modality because it helps stabilize the blood vessels and

protects the nervous system from critical damage during the surgery. However, the technique carries significant risk in recovery. For example, in CPB, exposure of circulating blood to the foreign surfaces of bypass machines can activate several inflammatory networks that severely impact the patient, and lead to critical heart failure and widespread inflammation, which contribute to early mortality in the fragile neonate/infant population [7, 8].

1.2 Low Cardiac Output Syndrome

1.2.1 Motivation

Although significant improvement has been made in reducing surgical-related mortality in pediatric cardiac surgeries, there is increasing evidence that a syndrome that commonly appears in surgical recovery contributes greatly to pediatric morbidity and mortality. Parr and colleagues are credited with the earliest description of such a syndrome in 1975, in a study where they observed that significant mortality directly correlated to low cardiac output states in pediatric patients [9]. Their observations led to the designation of the phenomenon as Low Cardiac Output Syndrome (LCOS), which is a collection of symptoms that may appear in surgical recovery. LCOS is associated with decreased cardiac output and tissue perfusion, metabolic inadequacy, and acute heart failure; it is the leading cause of morbidity and mortality in pediatric cardiac surgical cases [8, 9]. The decline in cardiac performance, and the resulting tissue oxygen imbalance, is common after CPB and it illustrates cardiovascular insufficiency and myocardial dysfunction in the patient [12]. Manifestation of LCOS is frequent in children under four years of age recovering from CPB. It appears in approximately 25% of this population and results in cardiac death in 20% of the LCOS cases [8,10–15]. Given that it appears in a quarter of postoperative cases and carries a high mortality rate, the focus of investigative efforts is in better LCOS identification to help mitigate its detrimental effects on survival and recovery. However, as of 2021, there is varied consensus on LOCS diagnostic criteria. This makes its identification and management more challenging for clinicians and motivates the need for the development of more universal and predictive criteria [7].

1.2.2 Clinical Presentation and Diagnosis

While no single biomarker and/or hemodynamic variable has been proven to statistically indicate LCOS with certainty, a common grouping of biomarkers monitored after cardiac surgery have been reported to be closely related to the incidence of LCOS. Of those, first, CO is a hemodynamic parameter that captures the overall volume ejected from the heart in one minute. Largely, the characteristic equation for CO is the patient's stroke volume (SV) in L times their heart rate (HR) in beats per minute (BPM) [11]:

$$CO = SV \times HR. \quad (1)$$

The CO is a reflection of cardiac performance and stability, as it documents the heart's ability to regulate blood pressure and tissue perfusion through modulation of SV and HR [19]. In LCOS, CO is decreased and is the source of the imbalance between tissue oxygen demand and supply. CO is a measure of cardiac performance because it is influenced by the preload, afterload, and contractility of the heart: factors that cause changes in the blood pressure and stroke volume, which drive end-organ perfusion [11]. Decreased contractility of the heart is a common outcome after CPB surgery due to myocardial ischemia (reperfusion injury) and systemic inflammation and is one of the most common causes of decreased CO, and potentially, LCOS [8, 10, 19, 20]. CO may be estimated from measured hemodynamic values or directly measured invasively with an in-dwelling venous catheter. In cases where stroke volume is not directly measured, CO may be calculated by using the systolic and diastolic blood pressures as a surrogate for SV in Eq. (1). This yields:

$$CO = \frac{((SBP - DBP) * HR * 2)}{1000 \text{ mL/L}}, \quad (2)$$

where SBP represents the systolic blood pressure (mm-Hg), DBP represents the diastolic blood pressure (mmHg), HR represents the heart rate (BPM), and the constant factor of 2 represents a normalization factor (mL/mmHg) [21]. Second, cardiac index (CI) is a reported hemodynamic variable in adult populations whose value is considered to reflect LCOS development, as it is a direct measurement of overall cardiac function [18]. However, CI is not typically monitored in the neonate/infant populations due to the invasiveness of its implementation. CI is directly related to the cardiac output (CO), as it is CO normalized to body surface area. Of the two parameters, CI weights the cardiac output against the total body surface area of the individual, thus making its evaluation of hemodynamic status more useful [22]. In the pediatric population, several investigations into the occurrence of LCOS and its associated hemodynamic markers have determined that a CI of less than 2.0 liters per minute per square meter (2.0 L/min/m^2) within the first 6-18 hours post-surgery suggests its presence [9, 13, 16, 19, 23]. However, in the event that the body surface area of the patient is unknown, CO may still be used in substitute for CI, and its normal range of 0.8-1.3 L/min in infants provides an alternative measure of cardiac output and performance. In addition, other

hemodynamic and clinical markers that are reported to be associated with the onset of LCOS are: decreased systolic blood pressure (< 90 mmHg or reduced by $> 20\%$), increased central venous pressure, increased systemic vascular resistance, tachycardia ($HR > 180$), weak peripheral pulses, oliguria (decreased urine output, < 0.5 mL/kg/hr.), hypotension, elevated blood lactate levels, increased arterial to venous oxygen saturation differences (> 30 points), decreased NIRS values, decreased mean arterial pressure ($MAP < 55$ mmHg), increased peripheral skin-to-core temperature differences, and an increased need for inotropic pharmaceutical support [8, 10, 11, 13, 15, 16, 20, 24].

A direct consequence of the imbalance between tissue oxygen demand and supply is the development of metabolic acidosis, which results from poor peripheral perfusion [19]. At the molecular level, decreased perfusion causes myocardial cells to switch from aerobic to anerobic metabolism, which produces lactic acid as a byproduct that induces metabolic acidosis [25]. Elevated blood lactate levels are considered an early sign of metabolic acidosis and are closely linked to changes in vascular tone (contractility), arterial blood pressure, and cardiac output [26]. Serum lactate levels greater than 2 mg/dL or rapid increases in levels is a clinically recognized sign of metabolic acidosis that is associated with the onset of LCOS [8, 19].

Another important marker of tissue perfusion status is the heart rate (HR). HR determines the extent of ventricular relaxation and perfusion. The period of time between each heartbeat is crucial for complete ventricular relaxation and contraction for optimal perfusion. If the HR is too high, coronary filling is insufficient and less blood is oxygenated than is required by the peripheral tissues and organs [19]. HR is optimally between 120-160 BPM for children under one year of age [27]. Tachycardic rates (> 180 BPM) are considered clinical signs of LCOS due to the relationship between HR and perfusion.

Central venous pressure (CVP_m) is another hemodynamic value associated with LCOS because it relates to cardiac output and preload [11]. CVP_m measures the pressure in the right atrium, which is influenced by the amount of blood circulating in the body and the relative compliance of the heart [28]. In critical care monitoring, this value becomes important when predicting the adequacy of cardiac output. The Frank-Starling mechanism is a basic principle in hemodynamics that describes the ability of cardiac myocytes to stretch, a process which improves the force of contraction during the heart cycle, and effectively increases the stroke volume. This adaptability provides the heart with a mechanism to help maintain normal cardiac output and blood pressure in the case of increased ventricular loads; however, in neonatal patients, this mechanism is not as effective [12]. Therefore, when CVP_m is elevated, the increase in preload overstretches the cardiac myocytes and decreases contractility and cardiac output. Since the heart is unable to increase its effective stroke volume, pulmonary circulation decreases [29]. CVP_m values greater than 15 cm H_2O , or about 11 mmHg, are considered clinically relevant signs of LCOS development [8].

Another clinical sign of LCOS development is increasing systemic vascular resistance (SVR). SVR is directly related to cardiac output because it measures left ventricular afterload and the heart's ability to increase stroke volume to overcome resistance from the vascular bed [9, 29]. Relatedly, CBP may alter the reactivity of the pulmonary and systemic vascular beds and increase SVR [12]. The heart's inability to push blood forward through the circulatory system results in a decrease in peripheral perfusion, a decrease in CO, hypotension, and an increase in myocardial work [31]. Abnormal SVR values can be assessed in two ways: 1. by percent increase with respect to baseline value (increase > 25 percent), or 2. by reference to a standardized range (2800-4000 dynes/sec/cm²) [12, 26]. SVR can be calculated from either measured and/or calculated hemodynamic values:

$$SVR = \frac{MAP - CVP}{CO} * 80, \quad (3)$$

where MAP represents the mean arterial pressure (mmHg), CVP represents the central venous pressure (mmHg), CO represents the cardiac output (L/min), and the multiplication by the constant 80 converts the units from mmHg/L/min to dynes/sec/cm⁵ [32].

Lastly, another central marker of cardiac performance and tissue perfusion is venous oxygen saturation (SvO₂) [33]. SvO₂ measures the oxygenation content of blood passing through the pulmonary artery or the superior vena cava, depending on where the catheter is placed, and can therefore measure insufficiencies in tissue oxygen supply and demand [34]. SvO₂ can help assess cardiac output because it depends on arterial oxygen saturation, the balance between systemic oxygen demand and CO, and hemoglobin levels. Simply, arterial oxygen saturation describes how much of the arterial blood is oxygenated and systemic oxygen demand describes how much oxygen is needed by the tissues. When oxygen demand is high, the rate of oxygen consumption typically increases to provide the tissues with adequate oxygenation. An increase in oxygen consumption can lead to an increase in CO to help provide oxygenated blood at a quicker rate in the systemic circulation to reduce the oxygen consumption rate back to normal levels [35, 36]. This relationship is defined by the Fick principle and helps describe the adequacy of oxygen delivery in the patient:

$$SvO_2 = \left[\frac{SaO_2 - VO_2}{CO} \right] \left[\frac{1}{Hb * 1.34} \right] \quad (4)$$

where SaO_2 represents the arterial oxygen saturation ($mL/min/m^2$), VO_2 represents the systemic oxygen demand ($mL/min/m^2$), CO represents the cardiac output ($L/min/m^2$), Hb represents hemoglobin count (g/dL), and multiplication by the constant 1.34 represents the oxygen content per gram of hemoglobin ($mL O_2/g$ of Hb) [35].

In LCOS patients, an increase in tissue oxygen demand is not readily compensated by an increase in CO, as CO is decreased in this population. As the demand for tissue oxygenation increases in this cohort, the lack of increased blood supply (due to decreased CO) results in an increased rate of oxygen consumption at the tissue level. Therefore, more oxygen is consumed in the systemic circulation, which lowers the amount of oxygen carried back to the heart from the tissues by the venous circulation (decreased SvO_2). A decrease in SvO_2 may also indicate metabolic acidosis, as values below 70% are correlated with the onset of anaerobic metabolism [37]. This finding is supported by Victor et al., who defined an increase in metabolic acidosis associated with decreased peripheral perfusion in LCOS patients [25]. A study presented by Rhodes et al. found that $ScVO_2$ values below 72% at admission were correlated with mortality in infants and neonates after cardiac surgery [36]. In this study, the catheter was placed in the superior vena cava, which is a technique termed central venous oxygen saturation ($ScVO_2$) that differs slightly from typical SvO_2 measurements. However, central venous placement may be more ideal for the sensitive infant and neonatal population, as it is a less invasive method for monitoring venous oxygenation [34].

Identification and management of LCOS is imperative in the pediatric population because the condition carries a significant risk of morbidity and mortality. Within the first three days of cardiac surgery, risk of heart failure and cardiac death is extremely high [38]. Patients who develop LCOS may also experience increased duration of mechanical ventilation, longer periods of intensive cardiac care and hospitalization, in addition to the higher risk of mortality [14, 20]. Given that no single clinical parameter exists to diagnose LCOS, postoperative monitoring of pediatric patients after cardiac surgery requires complex assessment of hemodynamic values and a thorough understanding of the pathophysiology of the syndrome. The rapid development of LCOS within the first 18 hours of recovery highlights the essential role bedside nurses play in identifying symptoms as soon as possible [10]. However, the lack of a central diagnostic criterion leads to disagreement amongst clinical care staff about the presence of LCOS and can delay intervention and management if little attention is paid to the trends of these hemodynamic values. Additionally, more invasive (but accurate) monitors for hemodynamic values may induce additional trauma to the patient and/or may be too expensive for routine clinical use and are, therefore, unavailable for assessment. However, more recent investigations into thermal profile trends have indicated that the temperature profiles in the core and peripheral regions may provide an early indication of metabolic

dysfunction and impaired organ perfusion. Potentially, this will provide a new avenue for developing a central criterion for the diagnosis of LCOS.

1.2.3 Etiology of LCOS

Many causes contribute to the development of LCOS in the postoperative period following cardiac surgery in pediatric patients and they arise from a variety of sources [13]. One of the biggest sources for the development of LCOS is the cardiac repair procedure itself, which utilizes CPB. CPB has the largest influence on LCOS development, as the body's natural response to the protective hypothermia entailed, and the inflammatory interaction between the subject's blood and the foreign surfaces of the bypass machine are two of the three major sources of LCOS. Essentially, CPB has been well-documented to cause widespread inflammation in patients through several mechanisms. One of the more obvious mechanisms is the inflammatory response caused by the physical procedure of oxygenating the blood through an external bypass machine and the exposure of the mechanically circulated blood to foreign surfaces of the bypass. Those interactions stimulate leukocytes, promote the release of endotoxins, cytokines, and oxygen-free radicals, along with that of other inflammatory mediators, despite the machine's sterility [11, 16]. The repercussions of CPB use continue as the inflammatory response can damage the pulmonary vascular endothelium and reduce nitric oxide (NO) production, which contributes to increasing vasoconstriction. The heightened expression of neutrophils damages the vascular endothelium by enhancing degradation of the basement membrane. More directly, the ensuing increased permeability in the vasculature can lead to capillary leak, edema formation, and hypovolemia. Reduced NO is also a negative effect of CPB, as the lack of NO disrupts the ability to maintain relaxed vasculature and ultimately leads to vasoconstriction [39]. As the immune system becomes widely activated following CPB, the body must supply increasing amounts of energy to additionally support the immune response, and so myocardial oxygen consumption also increases, thus, worsening the balance between oxygen supply and demand in peripheral tissues [8].

Additionally, the complement system response to CPB broadly activates the adrenergic system. The stimulation of the adrenergic system, in turn, upregulates epinephrine and norepinephrine, which are direct stimulators for vascular tone and heart rate, yielding an increase in vasoconstriction and tachycardia [12]. Both mechanisms contribute greatly to the source of cardiac and metabolic dysfunction in postoperative pediatric cardiac patients. Lastly, the restoration of normal flow in the blood vessels as the patient is transferred off the bypass machine can cause a phenomenon known as ischemic reperfusion injury (IRI). IRI is a majorly destructive condition characterized by widespread tissue necrosis and death. As such, it is a primary source of mortality in LCOS patients, because when compounded with intraoperative CPB effects, IRI can cause multi-organ failure [13, 33].

Other disruptions in the normal vasculature and hemodynamic values that can contribute to the onset of LCOS include: postoperative arrhythmias, residual shunts, intraoperative mechanical trauma, surgical stress, circulatory arrest, non-pulsatile pump flow, and re-warming of the patient after hypothermic CPB [12]. While no single indicator readily reflects the risk of LCOS developing, it is generally accepted that the contribution of multiple factors—such as systolic and diastolic dysfunction, heightened inflammatory response, and changes in cardiac load—can provide an estimate of LCOS occurrence [8].

1.2.4 Risk Factors for LCOS

While some of the causes of LCOS are well-documented and readily apparent, independent risk factors that directly correlate to the onset of the syndrome are not as defined. There is a slight gap in the literature that comprehensively and independently evaluates risk factors, but a few smaller retrospective analyses do provide some insights into some of the potential risks that are closely associated with LCOS. A study published by Bangrong Song, Haiming Dang and Ran Dong in the *Journal of Cardiothoracic Surgery* is the most recent attempt at deciphering clinical risk factors [8]. In their retrospective analysis of 283 CHD patients, they discovered that the patient's age, duration of CPB procedure (> 60 min), decreased pre-operative oxygen saturation (< 93 percent), and the presence of postoperative residual shunt or a two-way ventricular shunt independently predicted risk of LCOS [8]. These findings are supported by a larger, more comprehensive analysis performed by Xinwei Du et al., and published in *BMC Pediatrics* in 2020 [13]. Their study included 8,660 infants with CHD and documented almost 1,000 cases of LCOS developing after surgical repairs. The authors note that some of the more commonly reported risk factors for LCOS in adults include left ventricular ejection fraction (< 20%), increasing age, previous surgical history, and female gender; however, these values varied based on the type of surgical repair and the population studied. Du et al. found that age, circulation temperature, and aortic, atrial and ventricular shunts were independent predictors for LCOS, which supports the previous retrospective study on risk factors performed by Song et. al [13].

The elucidation of age as an independent risk factor for LCOS is particularly important, as the number of cardiac surgeries performed during the neonatal period continue to increase. Therefore, it is essential to understand how age affects LCOS risk and how to mitigate its effects to reduce LCOS in the younger fragile populations. Song hypothesizes that incomplete development of myocardial cells in younger patients make them particularly susceptible to hypoxia and ischemia [8]. Pediatric Intensivist Hari Krishnan provides a more detailed explanation of this susceptibility by noting that neonatal myocardium exhibits several characteristics that make it less resistant to some of the injurious effects caused by CPB [20]. Some characteristics include decreased sensitivity to insulin and increased dependence on glucose for

cardiac myocytes, resistance to inotropic medication, decreased mitochondria supply, and more permeable vascular barriers. Krishnan also notes that smaller-sized infants, coupled with more complex lesion repairs, and extended periods of aortic cross-clamping times and bypass indicate an increased risk of LCOS [10, 19].

1.2.5 Postoperative Management of LCOS

Several management techniques are employed clinically to help mitigate and prevent adverse effects from LCOS. The most important management tool for LCOS is early identification; by anticipating the onset of LCOS, the clinical team is able to mitigate and prevent the extensive damage caused by IRI and low cardiac output [15]. In order to optimally manage the patient's postoperative recovery, hemodynamic monitoring is widely used to determine cardiovascular function, tissue perfusion, effectiveness of inotropic agents, optimal settings of mechanical circulatory support and optimal ventricular loading conditions [7]. A thorough, systematic approach is necessary to evaluate and optimize these values and to consider cardiopulmonary interactions appropriately [20].

A large component of LCOS management is pharmaceutical support and intervention, particularly through the use of inotropic and vasodilatory medication. These types of medication can help improve tissue perfusion and regulate hemodynamic values, which can stabilize the postoperative recovery course [14]. Typically, inotropic support focuses on stabilizing preload values by improving myocardial contractility. When focusing on optimizing preload values, catecholamines are a standard inotropic agent selected for their ability to increase myocardial contractility and alleviate severe systolic dysfunction. Catecholamines act on the cardiovascular system through adrenergic and dopaminergic receptors to yield improved cardiac myocyte contractility and increased dilation of vascular smooth muscle cells. This two-part effect is accomplished by catecholamine's ability to stimulate the production of cyclic adenosine monophosphate (cAMP), which activates the adrenergic receptor pathway in both cell populations and results in the increased myocyte contractility and peripheral vasodilation [40]. The exact inotropic effect is largely dependent on the medication used and its dosage. Examples of catecholamines include dopamine, dobutamine, epinephrine, and norepinephrine with ranging effectiveness [16, 23]. However, usage of catecholamines can increase oxygen demand, HR, and risk of arrhythmia; therefore, more recent literature tends to favor the use of phosphodiesterase type III inhibitors for its lack of these limitations [14]. Phosphodiesterase type III inhibitors act on the cardiovascular system by increasing diastolic relaxation and myocardial contractility, which reduces preload, afterload, and systemic vascular resistance (SVR) [40]. These inhibitors specifically prevent the breakdown of cAMP in cardiac myocytes and smooth muscle cells, thus yielding its vasodilatory and contractility effects [7]. Milrinone is one of the more commonly

used phosphodiesterase type III inhibitors due to its effectiveness in improving cardiac index, decreasing filling pressure, reducing systemic resistance, and reducing risk of LCOS. However, dobutamine is less expensive than milrinone and is, therefore, occasionally used as a substitute [12, 16, 23]. In one of the largest randomized trials for a pediatric cardiac surgical population recorded to date, the use of milrinone improved hemodynamic values in patients already diagnosed with LCOS and reduced the risk of LCOS developing after surgery, this supports its more recent usage in acute clinical care [14].

Along with inotropic support, fluid administration and blood products are often administered to help improve preload values [9,10]. Inadequate preload may arise from surgical effects (blood loss) or from vasculature changes (capillary leak) and can lead to hypovolemia after cardiac surgery, and this may be augmented by fluid or blood product administration [12]. In order to maximize the effectiveness of fluid administration, small administrations are given over time to maximize preload values and cardiac output. Other management techniques for LCOS include delayed sternal closure (DSC), a surgical technique that delays the closure of the surgical site to mitigate abnormal intracardiac pressures and mechanical circulatory or ventilatory support, which supports non-stressed myocardial recovery [15].

1.2.6 Hemodynamic Monitoring

Along with hemodynamic value monitoring, serological markers of cellular hypoxia and peripheral perfusion are recorded to identify the onset of LCOS symptoms. Typical monitored values include: HR, systolic and diastolic blood pressure (SBP, DBP), mean arterial pressure (MAP), atrial oxygen saturation, atrial partial pressure of oxygen, oxygen consumption, peripheral skin temperature, hemoglobin, serum lactate levels, capillary refill time, arterial and mixed venous oxygen contents and differences, cardiac output, cardiac index, CBC panels, electrolyte panels, and regional oxygenation values [9, 13, 16, 32, 34]. The selection of which monitored values are consistently applied in the postoperative period depends on equipment availability, financial resources, and clinical expertise of each pediatric cardiac intensive care unit, and may differ between surgical centers. Selection of invasively monitored values, such as arterial and mixed venous oxygen content, may be preferred due to their accuracy, precision, and statistical validity; however, it is important to also evaluate the impact that invasive monitoring may have on the patient. Preference for noninvasive monitoring methods: e.g., near-infrared spectroscopy (NIRS), echocardiography, and peripheral temperature monitoring, may be a more suitable choice depending on the patient's overall cardiac status and stability. However, most centers use a combination of invasive and noninvasive monitoring methods. Reports on peripheral skin versus core temperature measurements have increased in recent years, as more sophisticated thermal tracking systems have become available. The technique is favorable because it is a dynamic, inexpensive, and noninvasive method to indirectly monitor

peripheral perfusion [9, 13, 35]. Overall, the evaluation of trends in the aforementioned monitored values can provide clinically relevant signs of early cardiac decline, and so consideration of trending multiple biomarkers simultaneously has been championed in recent literature. This approach allows the clinician to assess endothelial dysfunction, tissue injury, and inflammation more readily, which can assist in earlier identification of high-risk patients [12].

When selecting monitoring methods for trending analysis, it is important to consider the time scale. In some cases, the monitored values do not exhibit clinical significance until well after LCOS has been established. For example, serum lactate levels are considered the gold standard for measuring the degree of anaerobic metabolism and peripheral perfusion. However, this serological marker is a relatively late sign of cellular hypoxia and can show up hours after cardiac output has already decreased [7]. Measurement of decreased urine output, which can help indicate the status of peripheral circulation, is measured per hour and may also miss serial changes in hemodynamic values and cardiac index variables. While these values are clinically associated with LCOS, they are not considered good predictors of its development. Therefore, selection of monitored values must align with the goals of the trend analysis—whether it is in assessing independent risk, prognostic ability, or statistical association with the syndrome [15].

Additionally, other monitoring methods may be suboptimal choices for deciphering prognostic criteria for LCOS based on their invasiveness, cost, availability, and lack of standard reference values. For example, NIRS values, an indicator of regional oxygenation, below 58% have been reported to accurately assess and predict onset of LCOS with 100% sensitivity and 69% specificity; however, an additional study utilizing NIRS in the postoperative course directly refutes this statement. It reported that NIRS sensitivity and specificity were much closer to 48% and 67%, respectively, for decreased somatic values over 20% from baseline values. [9,36,37].

1.2.7 Core-Peripheral Temperature Gradients

Monitoring temperature gradients and thermal profiles in pediatric cardiac patients recovering from CPB surgeries represents a growing, yet still underutilized, field for noninvasive monitoring in critical care units. Peripheral temperature and its connection to peripheral perfusion, vasoconstriction, and cardiovascular status is supported by a history of literature dating back to the time of Hippocrates, where peripheral perfusion was established as a determinant of cardiovascular function [44]. While general temperature recordings became integrated into standard clinical practice shortly following the invention of the thermometer in 1871, there was not much investigation into quantifying changes in regional temperatures and their significance prior to the 1970s [45].

As noninvasive monitoring methods have greatly improved in terms of their portability, accessibility, accuracy, and limited impact to the clinical environment, the link between quantified skin temperature and peripheral perfusion has been investigated further for its use in predicting early symptoms of LCOS. As mentioned previously, hemodynamic assessment of some of the essential vital parameters associated with LCOS do not provide enough information about peripheral perfusion, nor do they act as good predictors for the syndrome as their clinically significant values lag behind the earlier warning signs of LCOS. However, noninvasive temperature monitoring methods provide the framework for earlier assessment of peripheral perfusion [46].

The peripheral temperature of the skin over time in critically ill patients has been previously verified as an index of perfusion and predictor of survival, and first gained notoriety in the famous Ibsen study in 1960 [47]. In this experiment, Ibsen demonstrated the link between peripheral temperature and cardiovascular status by inducing blood loss of 500 mL, which resulted in a decrease of 8° Celsius in the temperature of the great toe. Despite the decreased blood volume and skin temperature, no change in blood pressure was observed, which supported the hypothesis that peripheral temperature can detect peripheral vasoconstriction (and potentially, hypovolemic shock) in the absence of measured hemodynamic values. The replenishment of the 500 mL blood sample reversed the decrease in temperature, further supporting this conclusion [44].

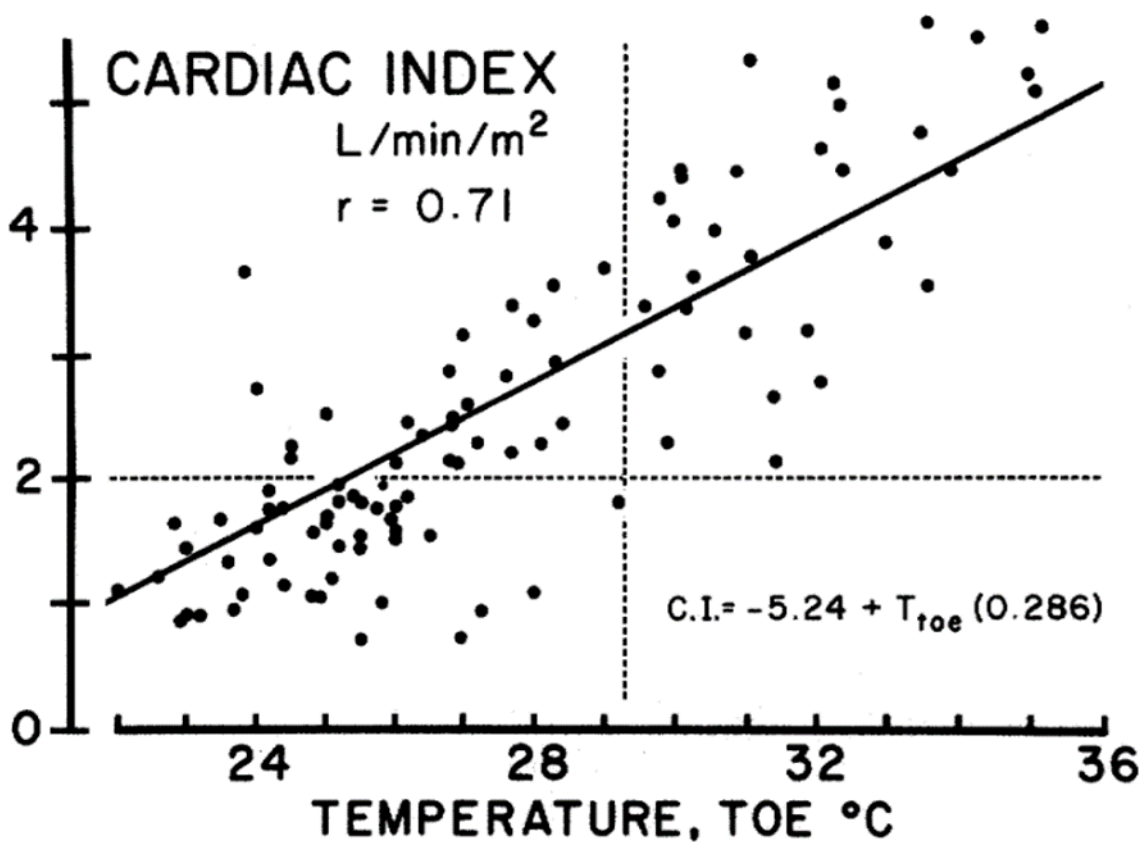


Fig. 2: Correlation between cardiac index and toe temperature, 100 sequential points, modified from [48]

In 1969, Henri Joly and Max Weil conducted a study on 100 patients in circulatory shock to quantify the relationship between skin and ambient temperature gradients and hemodynamic values [48]. It was hypothesized that since circulatory shock is clinically recognized by decreased blood flow after trauma or severe illness, the quantification of the temperature in the great toe could provide an objective measurement of the severity of shock. Joly and Weil were able to explicitly demonstrate that, in cases of declining cardiac index (<2.0 L/min/m²), the toe temperature would similarly decrease ($<27^{\circ}$ Celsius) in 95 percent of cases with depressed cardiac index, which quantified how peripheral temperature and cardiovascular performance may be related. The significant, linear correlation between the cardiac index and the great toe temperature quantified the relationship clearly: toe temperature was an accurate measure of peripheral perfusion and was directly correlated to cardiac output (Fig. 2). Since this finding, strong correlations have also been quantified between core and peripheral temperature gradients and cardiovascular performance in pediatric populations [37, 41].

Since the establishment of the relationship between peripheral temperature, perfusion, and cardiac performance, noninvasive thermal quantification methods have expanded to investigate how differences in core and peripheral temperatures may relate to cardiac function. In pediatric intensive units, core and peripheral temperature monitoring has been routinely used since the 1970s to monitor critically ill children [49]. Noninvasive measurements of the core and peripheral temperatures are particularly impactful in pediatric cardiac patients because they provide a quantitative assessment of cardiac function without introducing some of the morbidity, mortality, and costs associated with invasive pulmonary artery catheter assessment. The potentially fatal complications associated with invasive hemodynamic monitoring and its unreliable efficacy further highlights the need for noninvasive methods [50].

Investigation into the relationship between core and peripheral temperature differences and hemodynamic variables after pediatric cardiac surgery requires the definition of the average vasoconstriction and temperature values and their general trends that are part of normal CPB recovery. In literature, episodes of decreased cardiac output trigger a sympathetic neurohumoral response, which results in peripheral vasoconstriction and an increasing difference between core and peripheral temperature values. This response is thought to maintain blood pressure through peripheral vasoconstriction, resulting in a decline in peripheral temperature [38, 44]. In one investigation, Schey and colleagues compared the difference in the core versus the peripheral temperature values over time, a measurement they termed the core-peripheral temperature gradient (CPTG). Their investigation found that peripheral skin temperature was a better predictor of in-hospital mortality than MAP, a finding that was later supported in pediatric patients [38, 40]. Additionally, Schey and colleagues noted that decreasing tissue perfusion resulted in larger temperature differences between the core and peripheral regions and could be linked to poor cardiac function. The link between poor cardiac function, increasing CPTG, and peripheral perfusion is supported by the finding that intense vasoconstriction associated with increased vascular resistance resulted in cold peripheral skin [44].

While the temperature of the skin is affected by cardiac output, it is also affected by other hemodynamic factors, such as stroke index, urine output, and systemic vascular resistance [52]. The relationship between peripheral skin temperature and other hemodynamic factors provides a clearer assessment of the effect of management strategies and CPB side effects that can influence the CPTG size [44]. Continuous measurement of core and peripheral temperatures and calculation of the CPTG gradient is more desirable than serial measurements, as continuous measurement can reflect the dynamics of cardiac surgery and recovery more accurately [51]. Some investigations have shown that abnormal temperatures can precede or occur simultaneously with significant changes in hemodynamic values and further demonstrates the value of continuous temperature measurements [44].

Several studies have attempted to quantify the normal and abnormal trends in peripheral and core temperature and outline a general reference to assess the cardiac status of an individual. Briefly, an increase in the CPTG greater than 5° C is considered a sign of peripheral vasoconstriction and/or impaired cardiac output, as an increase in the CPTG value indicates a decrease in the peripheral temperature. CPTG values ranging between 2 and 4° C is considered the normal range during pediatric cardiac surgery recovery. Additionally, a consistent and sustained decrease in the CPTG within the first six hours was found to be predictive of normalizing serum lactate levels [37, 40]. In normal recovery profiles, the peripheral foot temperature ideally ranges from 32 to 34° Celsius and normalizes to this expected range from its baseline value within the first 6 hours of recovery. Cardiac index also exceeds 2.5 L/min/m² in individuals who do not show evidence of LCOS [40, 43, 45]. However, in abnormal recovery profiles, the peripheral foot temperature was less than 27° C at the 3 hour mark of recovery and likelihood of mortality was high [47]. An additional study of 70 pediatric patients after cardiac surgery discovered that peripheral foot temperatures in ventilated non survivors were significantly lower than in ventilated survivors at all time points in the first 24 hours of recovery [51].

Meskhishvili describes the course of an abnormal recovery profile in more detail and provides additional markers of LCOS that can be identified by the quantitative thermal profiles. In patients with LCOS, signs of decreased cardiac output, decreased cardiac index, tachycardia, arterial hypotension, and elevated systemic vascular resistance were apparent as early as 1.5 hours into the postoperative recovery period. These hemodynamic indications of LCOS were corroborated by the measured CPTG at the same time point; as this delta value was 11.9° C, the diagnosis of LCOS was confirmed to be accurate. Almost 20 percent of the patients diagnosed with LCOS did not survive; non-survivors also reflected increasing CPTG values with decreasing peripheral temperature values [52].

While the definition of CPTG and its expected values are defined thoroughly by the literature, confounding agents and limitations of noninvasive temperature assessment must be considered to ensure accurate analysis of thermal profile trends. Medication, such as vasoactive and inotropic agents, may influence hemodynamic and temperature measurements due to their effect on preload, afterload, and other hemodynamic variables. Additionally, the use of air-warming blankets in the critical care unit may also influence temperature measurements based on their proximity to the specified region [51]. The temperature profiles may also be influenced by the patient's age, weight, gender, length of CPB procedure, hyperthermic CPB value, and exposure to the ambient room temperature.

A 2015 study completed by Cuesta-Frau and colleagues investigated the use of a novel noninvasive thermal quantification device, with recordings of peripheral and core temperatures every 30 seconds in the first 24 hours of postoperative recovery. The increased frequency of temperature measurements was

hypothesized to be a more accurate indicator for predicting mortality (and LCOS) [53]. The collection of numerous temperature readings over the initial 6-hour period of recovery helped characterize patients with core-peripheral temperature normalizing early versus later than expected; the approximate CPTG during this time period was approximately 9.4° C in non-survivors and 3.7° C in survivors ($p < 0.0001$). The continuous measurement of the CPTG proved to be a more accurate predictor of mortality; if the CPTG was greater than 6.9° C, the odds of mortality were 140 times higher [47].

1.3 Medical Thermography

Since the mid-1800s, temperature has widely been regarded as an indicator of illness and changed hemodynamic status [54, 55]. The human body is typically homeothermic (uniform temperature), so changes in temperature in the core and peripheral regions are considered indicators of homeostatic imbalance. Various biological processes can affect the human body temperature, such as metabolic activity, vascular tone, circadian rhythm, and sympathetic and parasympathetic activity. Disruptions caused by disease, trauma, or other pathologies results cause a shift in this homeostasis, resulting in a change in temperature [56].

Typically, human skin temperature has been monitored using thermistors, thermocouples, and thermopiles placed on strategic skin locations, but the discovery of infrared radiation in 1800 by Sir William Herschel provided an alternative method to measure temperature in a noninvasive fashion [54]. The technology resides on the fundamental principle that all objects above absolute zero temperature emit some electromagnetic radiation, termed thermal radiation [57]. Within the electromagnetic spectrum, the wavelength of infrared radiation ranges between 0.75-1000 μm , with most medical investigations occurring between 8-15 μm [54]. The amount of thermal radiation, or spectral emission, is directly related to the temperature of the object measured and its emissivity. Emissivity is an important attribute to consider in thermal imaging, as it measures an object's ability (or inability) to reflect radiation. Emissivity values range between 0 and 1, where an emissivity value of 1 describes a blackbody, or an object that has no reflectivity. Blackbodies are known to radiate a continuous spectrum and to absorb all incident radiation, which are ideal properties for thermal imaging. The continuous radiation emitted by the object and absorption of incident radiation means that the measurement of the object's spectral emission is directly related to the object's true temperature [53, 56]. This relationship becomes clear with Stefan-Boltzman's law (Eq. 5), which calculates the emissive power of an object based on its emissivity and absolute temperature:

$$E = \varepsilon\sigma T^4 \quad (5)$$

where E represents the total emissive power of an object (W/m^2), ϵ is the emissivity of the object, σ is the Stefan-Boltzmann constant ($5.676 \times 10^{-8} \text{ W/m}^2\text{K}^4$), and T represents the temperature of the object (K) [54].

This thermal radiation can be captured by specialized cameras within the infrared spectral band and measure body temperature without physically contacting the body surface. The camera detector measures the amount of spectral emission at each spatial position within its field of view and translates the radiation into temperature values at each pixel in the obtained image. The resulting image, called a thermogram, describes the temperature recorded at each pixel in the frame. Human skin has an emissivity value of 0.98, which makes it a near-perfect blackbody; this emissivity value is constant across skin tones [54]. Therefore, thermograms can be produced accurately for skin temperature measurements in many populations, which forms the basis of its use in medical applications [57].

Initially, infrared thermal imaging methods were used for military purposes and were thus classified until as late as the 1950s, when the first medical thermogram was published [54-57]. Since the 1970s, interest in applying infrared imaging techniques in clinical settings has expanded rapidly due to the onset of computer image processing, which has allowed researchers to archive these thermal images and perform advanced quantification and analysis [58]. Given that the technique is non-invasive, non-contact, fast, harmless, and can monitor large areas simultaneously, medical thermography has been used widely to correlate thermal trends with clinical pathologies and diseases [56]. Medical thermography has been used to study the relationship between skin temperature and blood pressure, oxygen saturation, tumor and lesion identification, orthopedic injury, diabetic pathologies, rheumatic diseases, and to monitor critically ill and dying patients [54-56, 59, 60]. The accuracy of medical thermography has been extensively studied and found to be closely correlated with invasive thermal monitoring methods [61]. A 2021 study presented by Mostafa et al. compared infrared thermography to invasively monitored esophageal core temperature (the gold standard reference), and found that infrared thermography had the strongest correlation to true core temperature than other monitoring methods ($p < 0.001$) and specificity and sensitivity values above 90 percent for a wide range of temperature values [59].

When investigating neonatal and infant populations, medical thermography is particularly advantageous when considering their physiology. Their thin skin and low presence of fat mean that their measured skin temperature approaches their core temperature values, and that infrared imaging is as reliable and accurate as thermistors directly attached to skin [57]. Given that blood circulation is the principal mechanism of heat transfer in the body, investigations into thermal trends in the pediatric population can provide accurate and instantaneous assessment of circulatory status and document when circulation becomes abnormally disturbed [54]. Therefore, noninvasive infrared thermography is an appropriate

monitoring method for investigating LCOS, a cardiovascular-dependent syndrome that is heavily prevalent in pediatric postoperative environments.

1.4 Objectives and Aims

While the 2015 study conducted by Cuesta-Frau and colleagues provides a somewhat informative description of expected temperature profiles during recovery from pediatric cardiac surgery, it lacks comprehensive hemodynamic assessment and more extensive comparison between hemodynamic values and thermographic trends. Additionally, their noninvasive thermal quantification system had to be attached physically to the patient and is not completely free from the clinical plane (i.e., the bed of the patient).

In an effort to overcome some of these limitations and informational gaps in noninvasive thermal quantification protocols, the presented work describes the development of a novel, dynamic, and completely noninvasive thermal imaging system, with a corresponding temperature quantification protocol. The format of the work presented is influenced by the style of the Biomedical Optics Express Journal. The described system was capable of quantifying and identifying thermographic trends throughout the entirety of the clinical field of view. Thermal information was captured by a coupled infrared (thermal) and optical camera system that automatically sampled the clinical field of view every 30 seconds and stored the obtained images for later quantification and analysis. The primary aim of this work was to establish a routine protocol that could quantify thermographic data noninvasively obtained in a critical care setting. Children under 6 months of age were chosen for this investigation because of the high morbidity and mortality associated with LCOS in this population, and temperature monitoring has been suggested by the literature to predict LCOS earlier than monitored hemodynamic changes. The secondary aim was to analyze prospective case studies to identify thermal trends and potential relationships between the thermal trends and hemodynamic values to improve the identification of LCOS.

CHAPTER II

THERMOGRAPHIC QUANTIFICATION PROTOCOL

2.1 Clinical Study Deployment

The immediate goal of this study was to test IR-imaging based thermographic data analysis techniques that were developed to investigate the correlation between skin thermography and cardiac function following surgical repairs of congenital heart defects. Specifically, a normal and an abnormal recovery profile clinical case study of neonate/infant subjects was chosen for comparison to assess if skin thermography was capable of detecting suboptimal perfusion. This pilot study served as the foundation of a clinical protocol that investigated systemic perfusion via noninvasive IR thermography techniques in a pediatric population that was re-approved by the Institutional Review Board (IRB) in August 2020 to extend the study period into 2021. The approved clinical protocol is included in its entirety in Appendix A.

The investigative team was represented by the Principal Investigator (PI), Dr. Isaura Diaz, MD., a Board-certified Pediatrician and Pediatric Intensive Care physician at Vanderbilt Monroe Carrell Jr. Children's Hospital in Nashville, Tennessee. Dr. Justin Baba, PhD, a professor in the Biomedical Engineering Department at Vanderbilt University, with expertise in biomedical imaging and biophotonics, was a Co-Investigator of this study. All members of the investigation team were adequately trained, certified, and approved by the IRB committee prior to being granted access to any patient study information.

The study reported in this thesis was a standard Health Sciences investigation that began in August 2020 with an active enrollment lasting one year at the Monroe Carrell Jr. Children's Hospital at Vanderbilt, Nashville, TN. Under the direction of the investigative team, potential candidates for the study were identified using the inclusion criteria stated in the protocol. Two main qualifications were used to screen patients: age of the individual and post-operative admission into the Pediatric Intensive Care Unit (PICU). These two parameters were rationalized by the study aims and scope. LCOS is well-defined in the neonate and infant population; therefore, it was appropriate to limit participation to the referenced age group. Patients under six months of age undergoing a surgical correction of congenital heart disease were included in this criterion; patients older than six months or patients with purposefully manipulated temperature were to be excluded from the study population. Post-operative admission to the PICU was also a suitable qualification, as the patient would be able to be continuously monitored throughout the observational study and have immediate access to critical care, if necessary. Candidate selection was equitable and did not

restrict enrollment based on race, ethnicity, gender, or socioeconomic status. Before the patient reached the operating room, parents and legal guardians were provided with informed consent and anticipated benefits by key study personnel. They were reminded that their participation was voluntary and that they may have withdrawn at any time.

Two major aims defined the overall scope of the study data analysis and provided rationale for variations between routine post-operative care monitoring and the standards of care established by this protocol. The first aim sought to define a quantitative marker for LCOS based on the normal and abnormal, recovery profile clinical cases chosen to represent the neonate/infant subject population using noninvasive thermography. For this thesis, multiple parameters were assessed, including clinical, hemodynamic, and biochemical measurements of cardiac output and dysfunction. Cardiac output (CO), mean arterial blood pressure (MAP), systolic blood pressure (SBP), diastolic blood pressure (DBP), central venous pressure (CVP_m), heart rate (HR), mixed venous oxygen saturation (SpO₂), and systemic vascular resistance (SVR), were used to compare thermal trends against hemodynamic indicators of cardiac function and peripheral perfusion that are diagnostic for LCOS. This initial study establishes the basis for future evaluation of the hypotheses that thermographic data is an accurate evaluator of systemic perfusion and that it can be used to monitor oxygen imbalances in peripheral regions of the body. Therefore, as a first step, a representative standard of comparison needed to be defined for the future evaluation of this claim and this thesis serves to establish the initial baseline.

Tissue oxygenation was measured by a central venous catheter placed in the patient's pulmonary artery before surgery. The catheter was a flexible tube that can be used for hemodynamic monitoring, extracorporeal therapies, and venous interventions [62]. While this type of catheter provides critical access for clinicians to deliver medication and fluids, its placement is highly invasive and carries significant risk of complications. Recent literature supports an alternative catheter monitoring technique that is significantly cheaper and carries less risk than the current approach. In this method, the catheter was placed in the superior vena cava to monitor tissue oxygenation [63]. The IRB protocol specifies that a 4.5 French Edward LifeSciences PediaSat oximetry catheter is used for this purpose and is placed by the cardiac anesthesia team prior to surgery (Appendix A).



Fig. 3: Coupled Imaging System Mount

The second aim of the study was to preliminarily establish if thermographic imaging provides additional diagnostic information for potential inclusion in standard clinical practice. To support this claim, a noninvasive thermal imaging system was used to capture the patient's thermographic information. The imaging procedure generated thermographs, or heat maps, of the patient's body temperature over time. These images were analyzed to quantify temperature in specific anatomical regions and to identify key differences between the temperatures in different select regions of the body. In this study, a coupled thermal infrared camera and tablet system was used in clinical deployment. The IR-Pad 640 P Series Medical tablet, manufactured by Infrared Cameras Inc., was selected for its qualified imaging system, size, cost, and ease of clinical use among other factors [64]. The radiometric camera used was an uncooled focal plane array that captured 640 x 512-pixel thermal images in the 7-14 μm spectral band. The camera came pre-calibrated with respect to a NIST traceable blackbody radiation emission thermal source. The full technical specifications for the system are provided in Appendix B. The tablet system was mounted above the horizontal plane of the hospital bed by attachment to a Stryker articulating arm system (Fig. 3). Additional safety precautions included secondary fasteners that stabilized the attachment and prevented the system from falling.

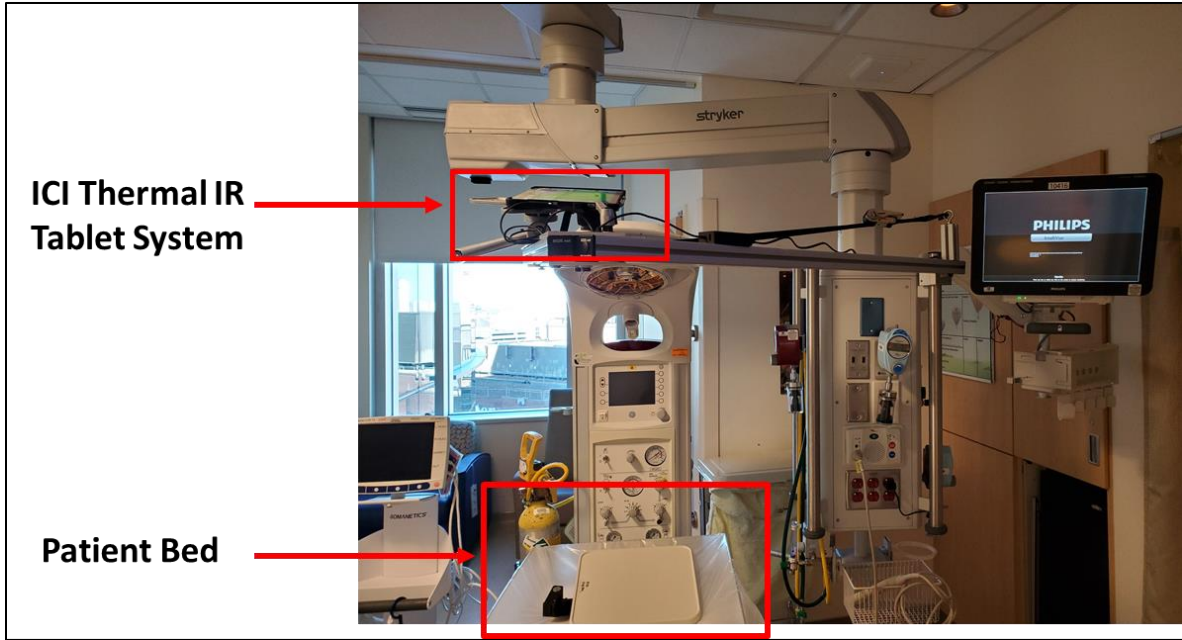


Fig. 4: Clinical Deployment of Coupled Imaging System

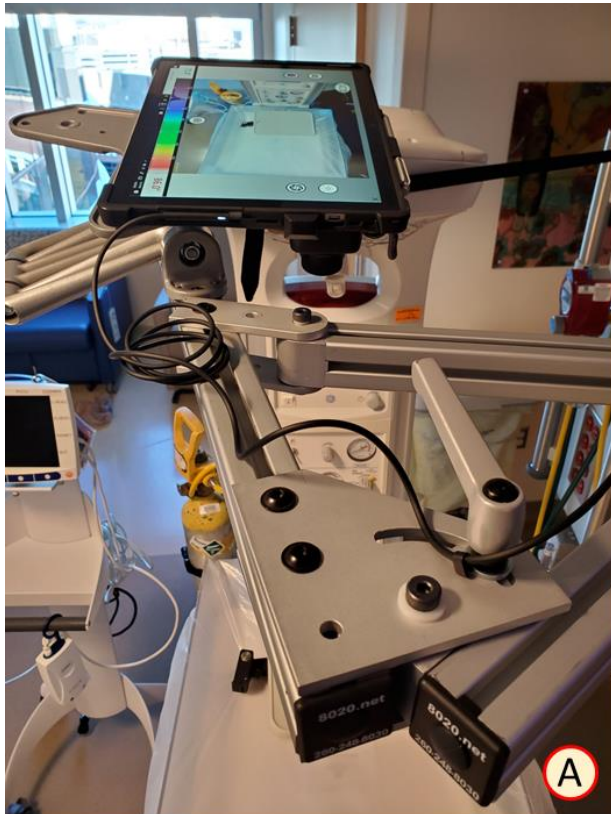


Fig. 5: Alternative Views- Clinical Deployment of Coupled Imaging System

Immediately after the corrective or palliative surgery, patients admitted to the PICU were externally monitored by a thermographic camera suspended above the hospital bed (Fig. 4,5). Thermographs were taken twice per minute for the first 24 hours that the patient remained in the PICU. In the beginning of the study, thermograph images included the entire uncovered body of the patient to provide an anatomical reference for image registration and processing techniques. This requirement was necessary to focus the heat information obtained from the thermographs to the appropriate anatomical location. After initial imaging, a minimum of one arm and/or one leg remained exposed to the camera system, but the patient was otherwise covered for the remainder of the study. At the conclusion of the 24-hour observation period, the system was turned off and the PI securely downloaded the study images and relevant clinical information. Study personnel informed the clinical staff of the study and provided a protocol for the immediate care staff (Appendix C) before the system was activated.

When participants were enrolled in the study, their information was stored in the Research Electronic Data Capture (REDCap) database. The database was maintained by the PI, as the obtained data includes Protected Health Information (PHI) and must always remain secured and may not be re-distributed to unauthorized users. Relevant clinical data was obtained from eSTAR, the Electronic Health Records (EHR) database used by the Vanderbilt University Medical Center network. All personal identifiers were removed before the study data was copied to an encrypted hard drive for image processing and analysis.

2.2 Processing Software

Table 1: Software Specifications

Name	Version	Developer	Customizations
			<i>Machine Learning and Deep Learning Toolbox</i>
MATLAB	R2020B	MathWorks	<i>Math, Statistics and Optimization Toolbox</i> <i>Image Processing and Computer Vision Toolbox</i>
Microsoft Excel	2016 (Build 14131.20278)	Microsoft Inc.	<i>Analysis Toolpack</i>
IR FlashPro	Beta Ver 0.83.3	Infrared Cameras Inc.	<i>N/A</i>

MATLAB is a computing environment that supports high-level image processing and was a suitable analysis tool for the described study. MATLAB version R2020b, developed by MathWorks, was used to execute most of the following software protocol. A proprietary software developed by Infrared Cameras Inc., named *IR FlashPro*, converted the thermographic images into the specified temperature scale. Additionally, Microsoft Excel version 2016 was utilized for data analysis and post processing methods. A complete list of software and technical specification is given in Table 1.

2.3 Software Procedure

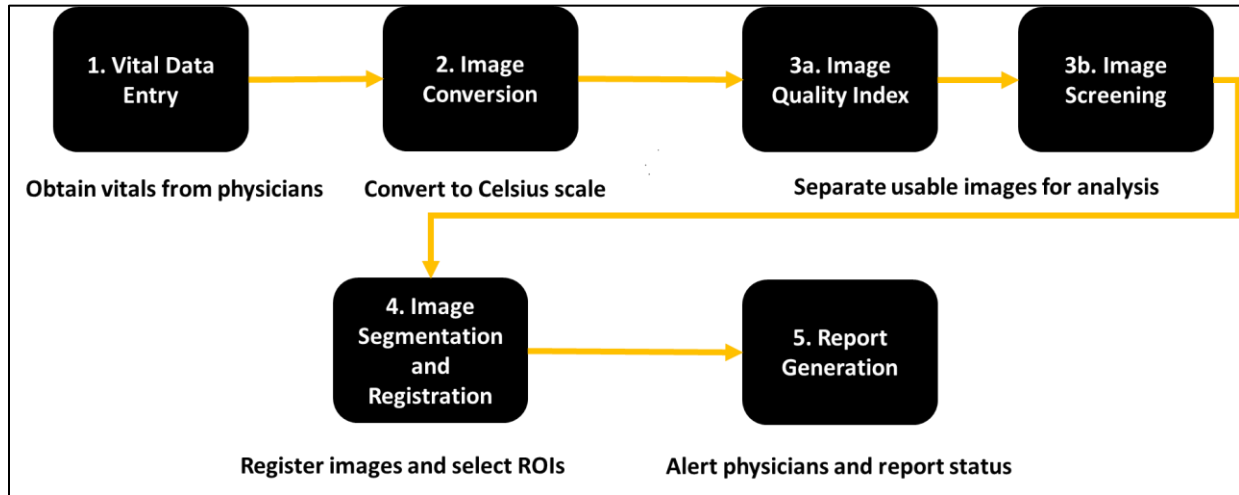


Fig. 6: Software Protocol Illustration

After the study data had been securely collected, stored, and encrypted, the thermal quantification protocol began. While the clinical deployment protocol was simple and effective, the software implementation for analysis was complex and multi-faceted. As a result, the thermal quantification protocol was separated into six discrete components to help simplify the aim of each analysis process and reduce the computational workload (Fig. 6). Individual protocols for each step of the software processing were produced and maintained throughout the study to establish consistent and repeatable analysis methods. In general, the analysis procedure began with the transcription of recorded hemodynamic values into a format compatible with MATLAB. Next, the thermographic information in the thermal images were converted to the Celsius temperature scale (from its default Kelvin values). All images were then screened for their eligibility for analysis, and eligible images were then registered together. After the images were manually segmented, report cards were generated for each image that captured the quantified thermal data, and these reported values were used to decipher thermographic trends and their correlation with hemodynamic data.

Besides the vital value transcription, the thermal quantification protocol took place in MATLAB (version 2020b). Three main scripts were coded to screen, register, segment, and analyze the study images. Any updates to the scripts were documented in the individual protocol and noted in the comments of the software code, per IRB standards. The final updates to the program scripts incorporated additional flexibility to help accommodate analysis spanning multiple dates and included additional dialog options for the user to return to previous analysis and study folders to maintain analysis continuity. Flexibility in the

software was an essential accommodation due to the rigorous and demanding nature of manual image segmentation and registration, which took upwards of several uninterrupted days to complete. Updates to the MATLAB script allowed the user to pause and resume segmentation and analysis at any time, which helped reduce user fatigue and maintained data privacy and security for the study, as the program was no longer required to run continuously.

2.3.1 Vital Data Entry

The first step in the analysis of the thermographic data obtained in the clinical study was to transcribe vital hemodynamic information recorded during the 24-hour observation period into a MATLAB-compatible format. The vital values were entered into an Excel file and exported as a tab-delimited text file for the MATLAB analysis procedure. Typically, vital information was recorded every minute of the observation period. For a 24-hour study, this corresponded to 1,440 lines in an Excel file and roughly 8,600 unique entries in total.

Table 2: List of Recorded Vital Values

Recorded Vital Value	
1.	Hour
2.	Minute
3.	HR (heart rate)
4.	SpO ₂ (oxygen saturation)
5.	SBP (systolic blood pressure)
6.	DBP (diastolic blood pressure)
7.	MAP (mean arterial pressure)
8.	CVP _m (central venous pressure)

The vital information was conferred to the research team via PDF format with all personal identifiers removed. Only one hospital was included in the described study, but vital monitoring differed slightly between study cases. After discussion with the clinical care team, it was determined that eight values were to be transcribed from the provided vital data sheets. The complete list of vital values is included in Table 2, with their acronyms as they appear in the original file preceding their description.

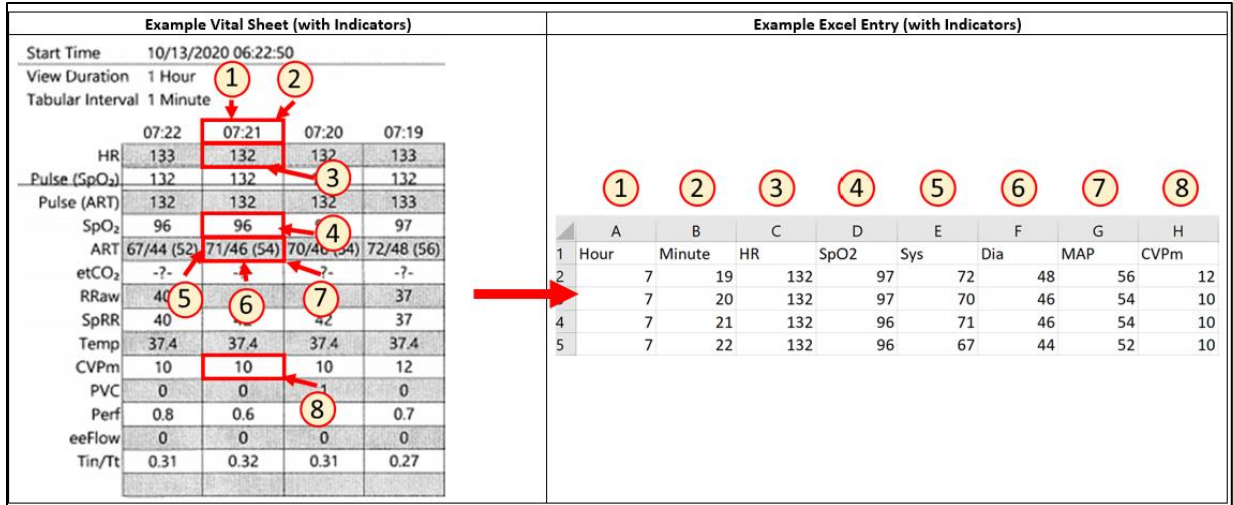


Fig. 7: Example Vital Sheet and Excel Entry

The data was copied over from the soft PDF copy into an empty Microsoft Excel file with eight headings matching the list described previously. The next portion of the procedure was to copy over each corresponding vital value, beginning with the earliest time point, exactly as they appeared on the page, into the corresponding column in the Excel file. If no value was listed for any given parameter, “NaN” was entered as a placeholder for the missing value. Once all entries had been completed, the Excel file was compared with the original PDF copy to verify its accuracy before it was exported to the tab-delimited text file format for later use (Fig. 7).

2.3.2 Image Conversion

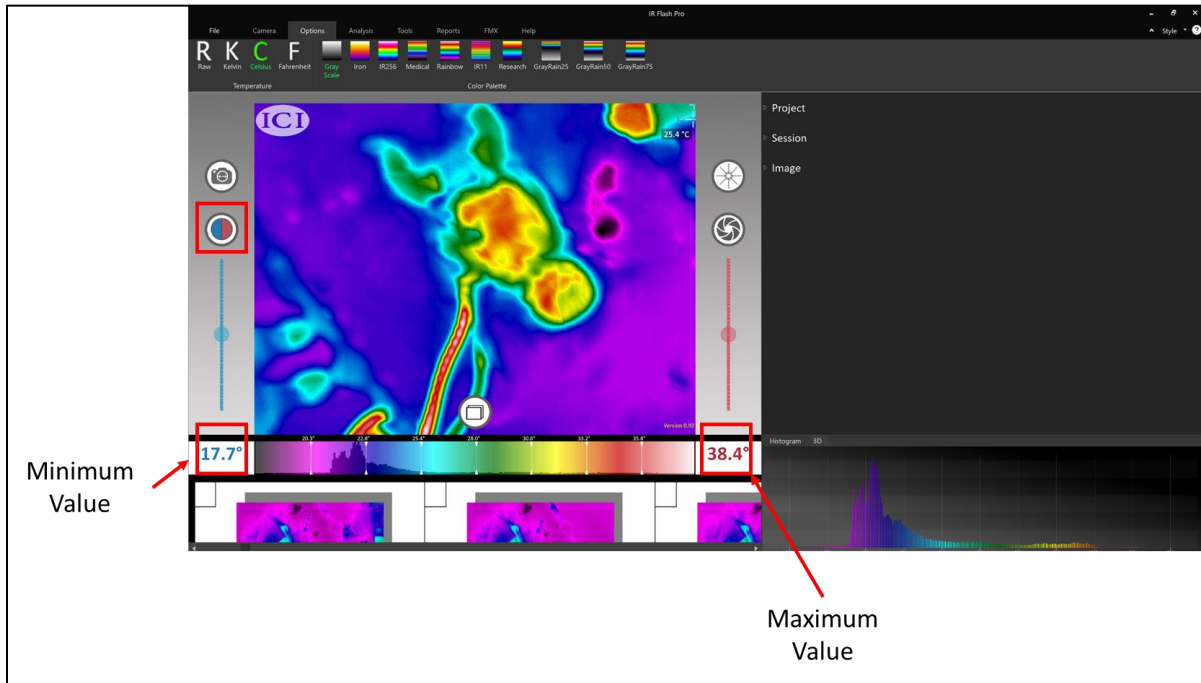


Fig. 8: Editing Temperature Axes

Before the obtained study images were registered and segmented in MATLAB, the thermal images were pre-processed in IRFlashPro to re-map the default temperature scale from Kelvin to Celsius. IRFlashPro is a software produced by the thermal camera manufacturer that provided the ability to change the displayed temperature units for clinical evaluation. Additionally, the minimum and maximum temperature values were edited to reflect the expected clinical values, which adjusted the gradation of the temperature scale to a more appropriate range (Fig. 8). The minimum temperature value was set between 17.5° and 20.0° Celsius, as this was below the expected ambient temperature and provided the most contrast between the subject and the background. The maximum temperature value was set between 37.5° and 40° Celsius, as patients were not expected to exceed 40° Celsius in temperature during the study as it corresponds to extreme fever. The temperature scale was applied to all thermal images in the study, and the adjusted images were exported in tagged image file format (.TIFF), a format known for high image quality and compatibility with MATLAB programs.

2.3.3 Image Quality

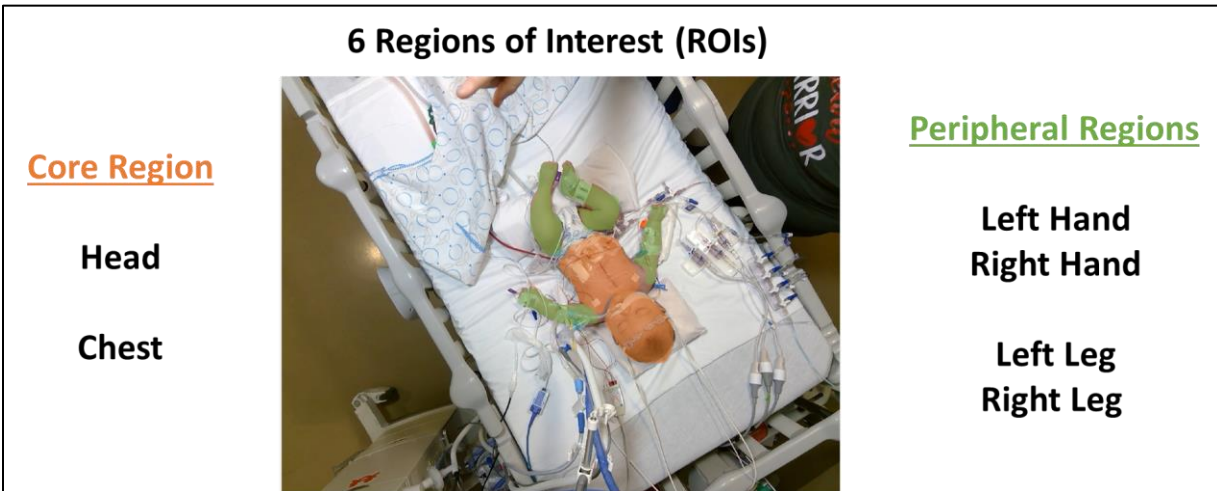


Fig. 9: 6 Regions of Interest (ROIs)

The basis for the image quality index procedure was rooted in the identification of the six primary regions of interest (ROI) for thermographic analysis. The head and chest region of the patient formed the core reference, and the patient's limbs formed the peripheral reference for the analysis (Fig. 9). Ideally, all six regions would be visible throughout the entirety of the study and each region's thermal trends could be compared over time. The selection of the six ROIs were consistent with the core and peripheral definitions present in the literature (see Chapter I).

Each image captured by the described system could not be used for analysis due to interruptions in the clinical protocol that resulted in obstructed or confounded views of the patient in the postoperative care unit. Routine postoperative monitoring and care procedures, such as echocardiogram and electrocardiography exams, medication administration, positional adjustments, and hygienic care were expected, as they are standard practices in critical care medicine. However, these procedures briefly interrupted the system's field of view of the patient and rendered affected frames ineligible for thermographic analysis due to the presence of confounding external thermal factors and physical obstruction of the view of the patient. Additional interruptions included patient visitors, warming blankets, medical equipment, and comfort coverings (such as socks, headbands, and hats). Due to the variability of the obtained clinical images, screening of the study images was required to eliminate frames that could not be used for thermographic analysis and to retain optimal samples for image registration and segmentation.

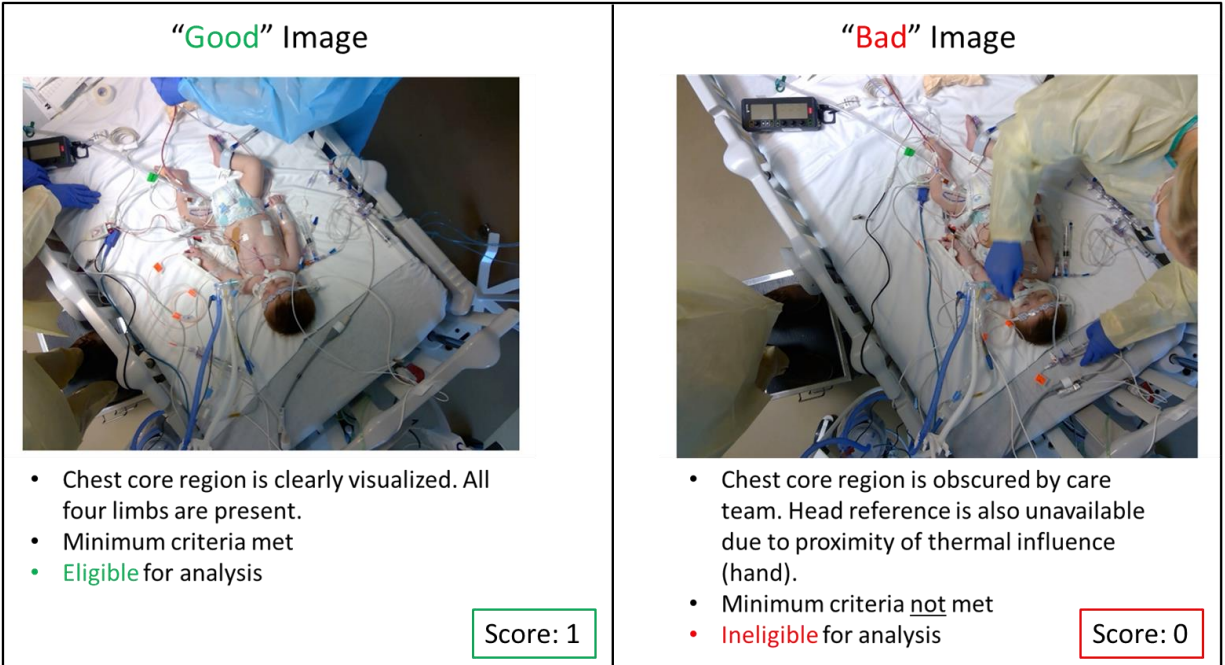


Fig. 10: Comparison Between "Good" and "Bad" Images

Images were scored for analysis on a binary scale, where a "1" score represented a "Good" image, and a "0" score represented a "Bad" image that could not be used for analysis. The scoring was determined based on the following minimum criteria: the patient's chest and at least one peripheral limb must be clearly and completely visualized with distinct boundaries, and no object, person, or equipment may obscure these regions. The patient was also required to be completely in frame, although a complete view of the hospital bed was not required. If the image met the standard, it was rated as a "1" and included in the thermographic analysis; if the image failed to meet the described criteria, it was rated as a "0" and excluded from analysis (Fig. 10).

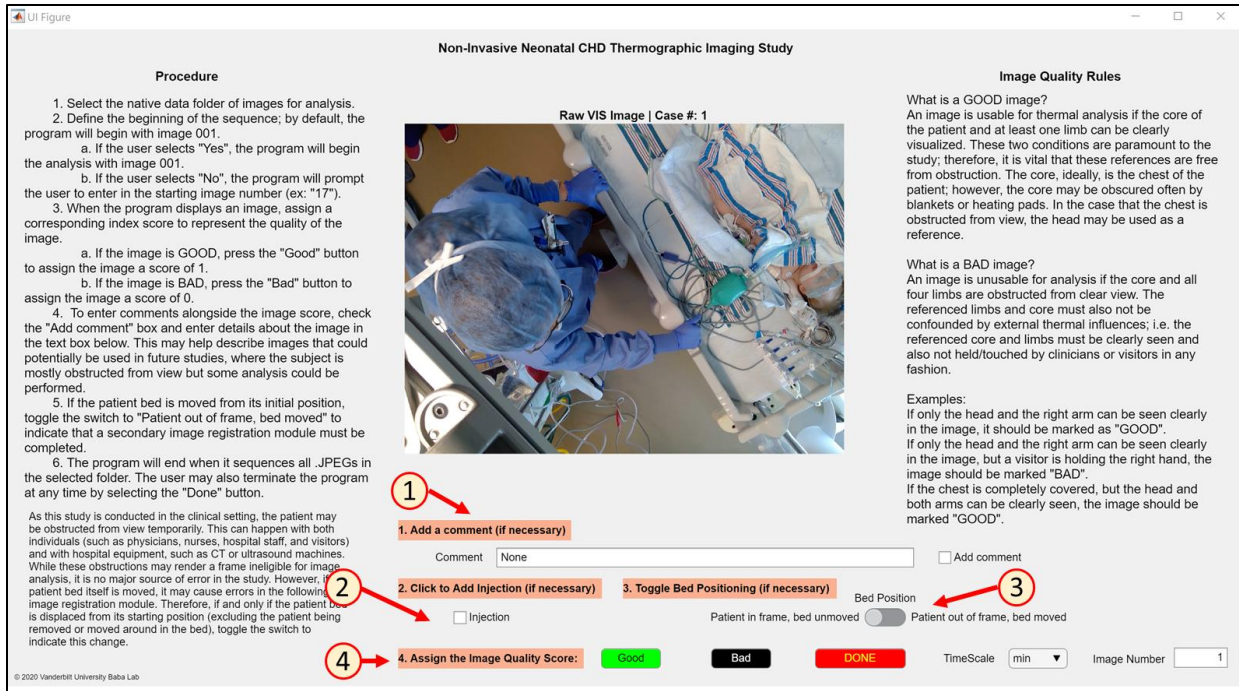


Fig. 11: Image Quality Application Steps

A MATLAB application was constructed to sequence through all images in the study and to assign the quality score and additional comments to each image (Fig. 11). Supportive text in side panels of the application outlined the general procedure for the quality scoring and provided additional details about confusing images to maintain the repeatability and consistency of image scoring. In general, four steps were completed for each image: attach individual comments (if necessary), record a visualized injection, designate bed positioning, and assign the final image score. Individual comments were used to help identify borderline images, and injection recordings were used to identify potential influences on the thermographic data later in the analysis procedure. Bed positioning was recorded to help determine when image registration needed to be repeated; if the bed did not move in the frame over the course of the study, a repeat of image registration was not necessary. Lastly, the final score for the image was recorded and stored in a text file with corresponding study information to be used in the image registration and segmentation procedure. Once a score was attributed to an image, the program automatically sequenced to the next image in the study, and the process was repeated until all study images were scored.

2.3.4 *Image Registration and Segmentation*

The next portion of the quantification procedure contained two subparts: image registration and image segmentation. These two parts were contained in a singular MATLAB script file that allowed the user to manually register the infrared and optical images together and to segment the registered optical images to obtain thermographic data from the selected region. A typical timeframe for this portion of the procedure was upwards of seventy hours of uninterrupted work to manually segment a complete set of study images. All image registration control points and segmentation masks created in this procedure were saved for potential AI modeling and training in the future.

Image registration was performed using multimodal analysis methods in MATLAB version 2020b. The Control Point Registration Tool, as part of the Image Processing Toolbox, provided a non-rigid feature matching-based transformation between the optical and infrared images using manual control point selection and local weighted mean-based interpolation to match the paired images together [65, 66]. A non-rigid transformation method was chosen to alleviate the local distortion between the infrared and optical image, an intrinsic difference between the two systems due to differing magnifications and field of view offset. A non-linear median filter and a Gaussian filter were applied immediately before the registration step to pre-process the image and to reduce image noise [67, 68].

In the registration procedure, the user identified an optical and an infrared image pair for registration. The optical image chosen for registration had clear, unobstructed view of the individual with all four limbs, the head, and the chest visualized in the frame completely. Once the user had determined what optical image was appropriate for registration the user selected *both* the VIS (optical) image *and* the IR (infrared) image for the Control Point Selection tool in MATLAB.

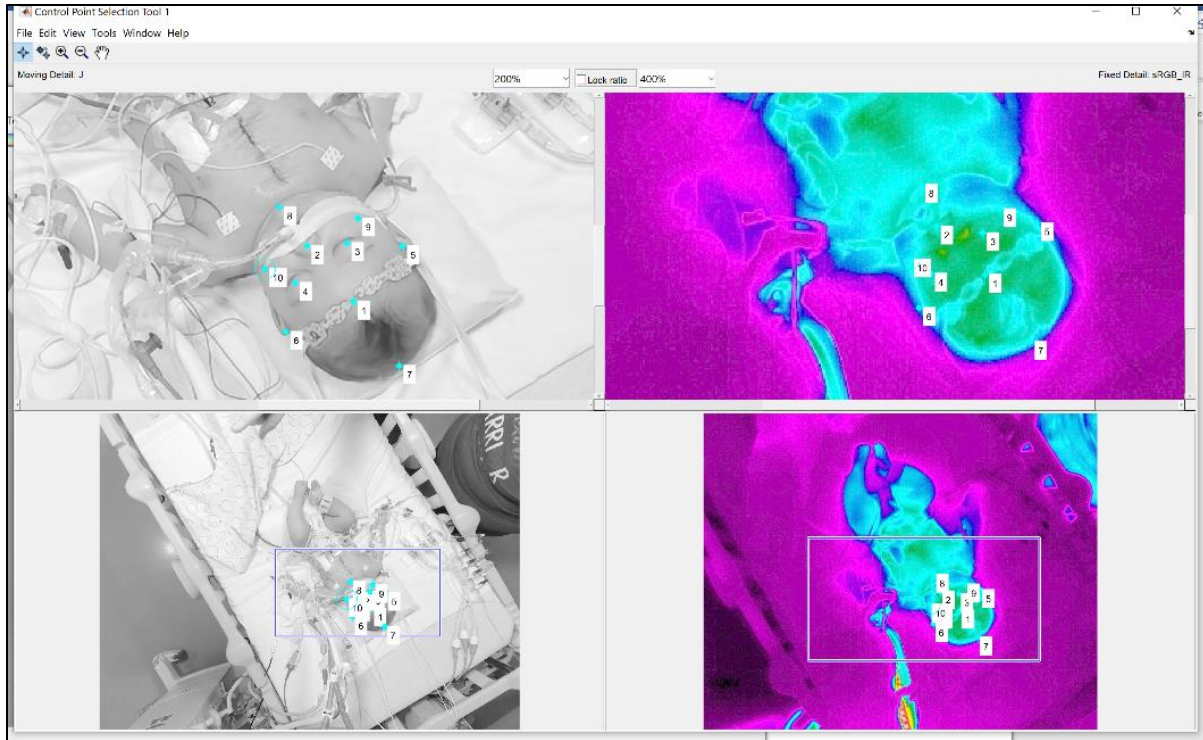


Fig. 12: Image Registration Control Points- Head

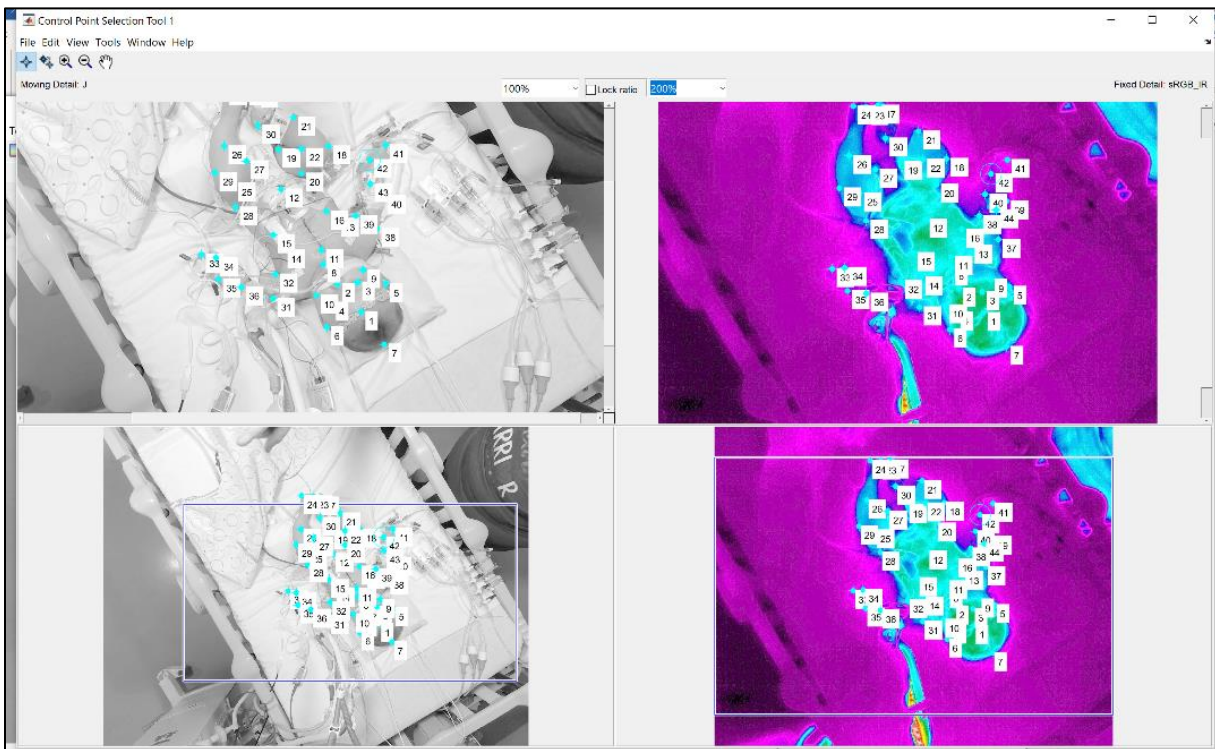


Fig. 13: Image Registration Control Points- Body

Once the user had designated which pair of images to use in the registration protocol, the Control Point Selection Tool opened and allowed the user to designate landmark features to register the infrared (IR) image to the visual (optical) (VIS) image. Appropriate landmark features included the eyes, ears, nose, mouth, hands, feet, arms, fingers, and toes. The registration was performed by identifying landmark anatomical features in the reference (optical) image, and then by matching the approximate location of the same anatomical feature on the sensed (infrared) image. A minimum of 10 control point pairs per anatomical region was used to fully define each region of interest; approximately 60 control point pairs were used to fully define the study images. When an error was made in feature identification, the user adjusted the control point to be accurately positioned before moving on to select the next registration control point pair. The pairing process was repeated until the entire anatomical structure of the patient was defined on both images using the pairing system. A minimum of ten training points were expected in each anatomical region, with an overall goal of forty to sixty training points to define the subject in its entirety. Regions of interest included the head, chest, right arm, left arm, right leg, and left leg (Fig. 12, 13).

Once all control points had been satisfactorily selected, the program exported the control pairs to the workspace and applied a local mean-weighted, non-rigid geometric transformation between the optical and infrared image to produce the final, registered image. The registered image was checked for anatomical accuracy before beginning the manual segmentation procedure. Analysis and data log files were generated at the completion of image registration and updated continuously throughout the segmentation procedure to detail the user, date, time, study data, and system information to maintain documentation requirements for the IRB study and to provide continuous monitoring of the study analysis.

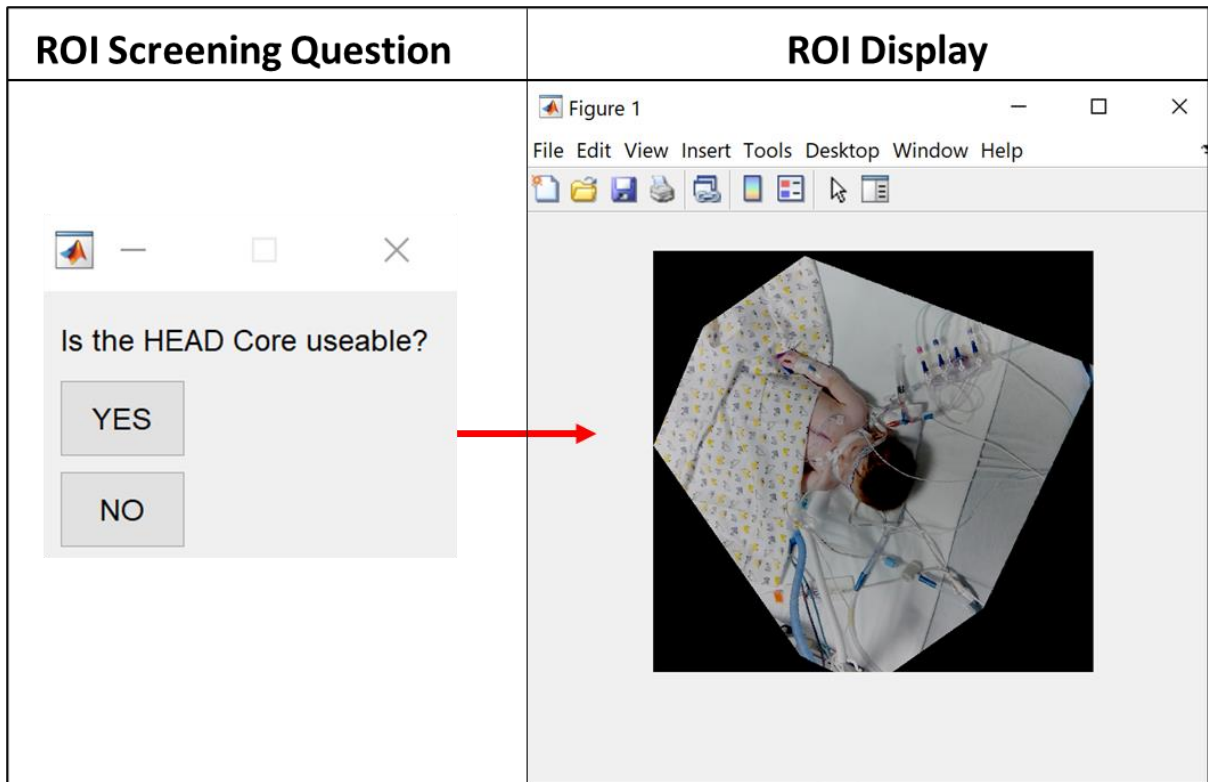


Fig. 14: ROI Screening Query

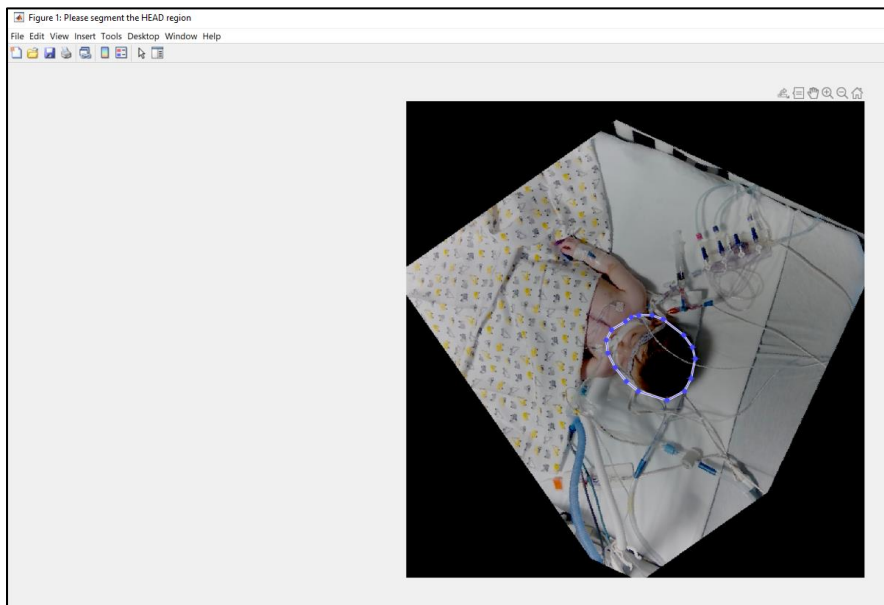


Fig. 15: Example ROI Selection

Manual segmentation was performed in MATLAB by implementing user-defined polygons on the registered images to define the region of interest (ROI) for all six regions identified in the image quality procedure. A preview of the registered image was shown before segmentation to check for its availability for analysis (Fig. 14). Each ROI was outlined on the registered image using MATLAB's free-form polygon selection tool to define the region completely and accurately for all registered images in the study (Fig. 15). ROI definition was performed in sequence, beginning with the head region, and proceeding through the chest, left leg, right leg, left arm and right arm in sequence for each image. After each region was defined, a preview of the resulting mask was displayed and checked for its accuracy before defining the next region on the image. The thermographic data in each region was calculated by applying each ROI mask to the registered thermal image to obtain all temperature values at each point in the mask-defined region; the mean, standard deviation and standard error were calculated for each region and comparisons between the core and peripheral regions were also calculated to provide instantaneous assessment of thermographic trends.

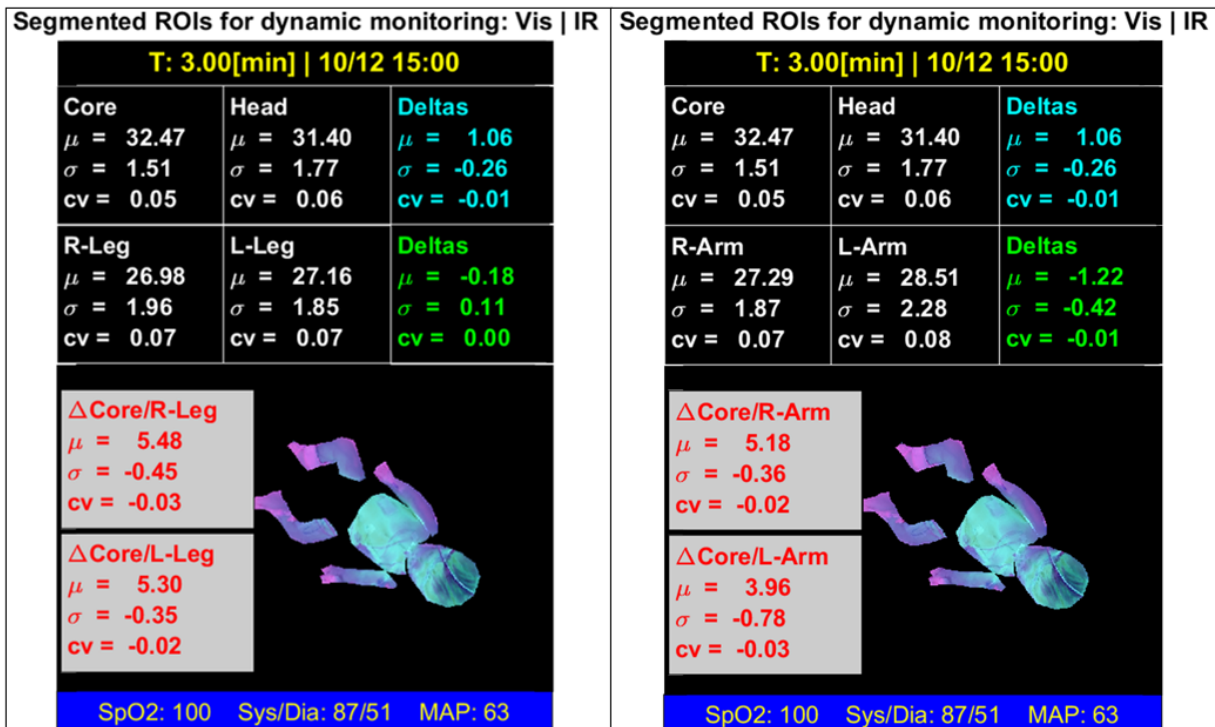


Fig. 16: Typical Thermographic Report Card

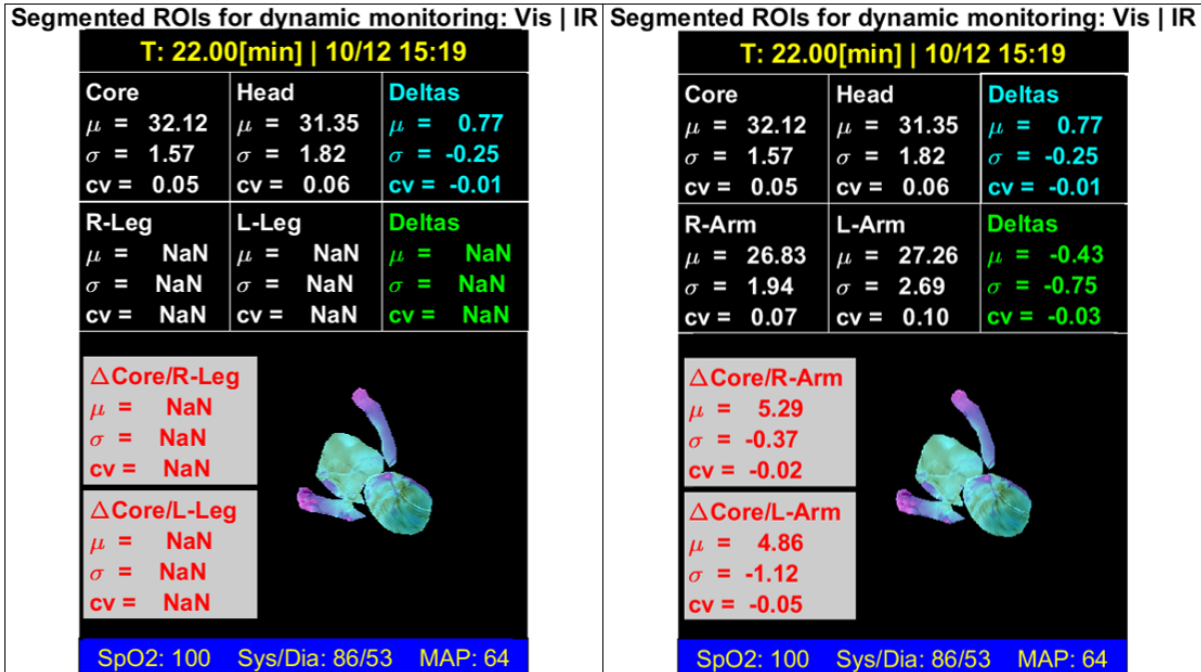


Fig. 17: Incomplete Thermographic Report Card

After the thermographic data had been calculated for all available regions in the study image, two report cards were generated to outline and display the calculated thermographic values, corresponding hemodynamic data, and a visual thermal representation of the subject at the study time point (Fig. 16). The visual representation of the subject was generated by displaying the user-defined ROIs on the thermographic image to provide a visual illustration of the patient's temperature. In cases where regions were unavailable for segmentation, the report card was still generated, but with "NaN" listed in fields where the value could not be calculated (Fig. 17). After the report cards were consulted for accuracy, manual segmentation of the next registered study image began, and the process of defining the six ROIs for each study image was repeated completely until all available images in the study were completely segmented for the patient.

2.3.5 *Post Analysis Processing Methods*

Analysis of the obtained thermographic data was performed in MATLAB and Excel to evaluate thermographic trends and to evaluate correlations with monitored hemodynamic values. The statistical considerations and expected outcomes are described completely in the IRB protocol (Appendix A). Briefly, the thermographic data was evaluated alongside other clinical markers: heart rate (HR), cardiac output (CO), systemic vascular resistance (SVR), mean arterial pressure (MAP), systolic blood pressure (SBP), diastolic blood pressure (DBP), central venous pressure (CVP_m), and oxygen saturation (SpO_2). Although central venous oxygen saturation ($ScVO_2$) was measured in the clinical environment, its values were not reported in the vital data, and so its value unfortunately could not be compared to thermographic trends. The basis of the analysis relied on the demonstrated literature that a potential predictive marker for LCOS was an increasing differential between the peripheral and core temperature values. As the difference between the limb temperature and the core temperature increased clinicians considered early development of LCOS and evaluated the patient to see if additional care was needed and to observe if there were significant changes in hemodynamic values. Therefore, the thermal trends in each region were charted, along with the comparison between core and peripheral temperatures, to help ascertain the connection between temperature and hemodynamic values.

CHAPTER III

CASE ANALYSIS AND DISCUSSION

3.1 Pilot Study Analysis

Two case studies were chosen for analysis based on three main criteria: completeness of image capture (at least 24 hours of image capture and recording), record of monitored vital values (either by minute or by hour), and quality of captured images (>40% of obtained images eligible for analysis). Based on these criteria, less than eight case studies were eligible for the thermal quantification protocol. The first case study was chosen to investigate a “normal” recovery profile after congenital heart defect (CHD) surgery utilizing cardiopulmonary bypass (CPB), and a second case study was chosen to inform on “abnormal” recoveries in the immediate postoperative period. Analysis of both case data, which were obtained through a Vanderbilt University approved IRB protocol (see Appendix A), was performed according to methods described in the previous chapter (Chapter II).

3.1.1 Case 1: Background

For the first case, the subject was under six months of age and recovering from CHD correction that utilized hypothermic CPB repair. No major clinical events were recorded for this subject in their postoperative recovery. This makes its thermal analysis useful for baseline comparison and helps to establish the normal recovery profile for this population. Following this procedure, the core-peripheral gradient was expected to decrease over the first six hours of the study, and peripheral temperatures expected to increase from baseline values in the same time period (see Chapter I, subsection 1.2.7). Normalization of the core temperature to 32-34° C within the first six hours is expected in normal recovery profiles. The corresponding optical and thermal images were obtained using the previously described thermal imaging system (see Chapter II), along with their monitored vital values that were recorded each minute throughout the study.

3.1.2 Discussion

Table 3: Observed and Calculated Hemodynamic Monitoring Values (Case 1)

Observed and Calculated Hemodynamic Monitoring Values (Case 1)																
Hour	Oxygen Saturation (SpO2) (%)		Systolic Pressure (mmHg)		Diastolic Pressure (mmHg)		MAP (mmHg)		HR (BPM)		Central Venous Pressure (CVPm) (mmHg)		Cardiac Output (L/min)		Systemic Vascular Resistance (SVR) (dynes/s/cm ²)	
	Mean	SD	Mean	SD	Mean	SD	Mean	SD	Mean	SD	Mean	SD	Mean	SD	Mean	SD
1	100.0	0.0	78.2	5.5	54.5	3.4	62.1	4.0	151.0	1.5	11.2	1.5	0.7	0.1	5849.3	459.7
2	98.7	1.1	71.2	2.3	50.7	1.4	57.3	1.6	148.0	0.7	10.6	0.6	0.6	0.0	6184.8	295.0
3	96.1	1.1	70.0	3.8	50.0	2.8	56.3	3.1	147.6	1.4	12.3	1.8	0.6	0.1	6099.2	599.0
4	97.1	1.3	76.9	4.0	54.6	2.4	61.8	2.8	150.8	1.0	12.1	1.9	0.7	0.1	5939.2	318.0
5	97.1	0.9	74.7	3.8	52.7	2.4	59.9	2.9	151.4	0.8	11.7	2.7	0.7	0.0	5798.5	294.6
6	96.1	0.7	69.0	3.2	48.2	2.2	55.2	2.3	144.5	4.7	11.1	1.9	0.6	0.1	5917.5	497.9
7	94.3	2.4	75.6	4.3	50.7	2.4	59.2	2.6	125.8	5.8	14.3	3.0	0.6	0.0	5766.9	423.2
8	94.9	2.5	76.9	3.5	50.6	2.3	59.3	2.8	122.4	0.7	11.5	1.2	0.6	0.0	5944.2	289.4
10	94.4	1.9	68.8	4.3	45.3	2.4	52.9	3.1	122.9	0.7	10.2	1.5	0.6	0.1	5936.4	277.9
11	93.9	2.0	77.8	2.5	49.7	1.4	59.0	1.8	123.8	0.8	10.0	1.5	0.7	0.0	5644.3	322.6
12	92.9	1.4	69.3	5.4	45.7	3.4	53.4	4.5	124.0	1.1	8.8	1.3	0.6	0.1	6108.5	267.0

Table 3 highlights the measured and calculated values from the pilot study, including key hemodynamic monitoring criteria and estimated cardiac output [21]. Here, SD stands for the calculated standard deviation. In terms of critical hemodynamic values, the subject largely falls within the control ranges and did not display significant markers of impaired cardiac output. The reported oxygen saturation for the subject was higher than expected (>90%) and indicated that the subject was well perfused. The systolic and diastolic blood pressure (DBP) values also fell within the expected range; although the systolic blood pressure (SBP) was slightly depressed in comparison to control values, it did not exceed a 20% drop from its average value, which is an acceptable amount of variation. The mean arterial blood pressure (MAP) and heart rate (HR) values also fell within expected ranges and indicated good cardiac performance.

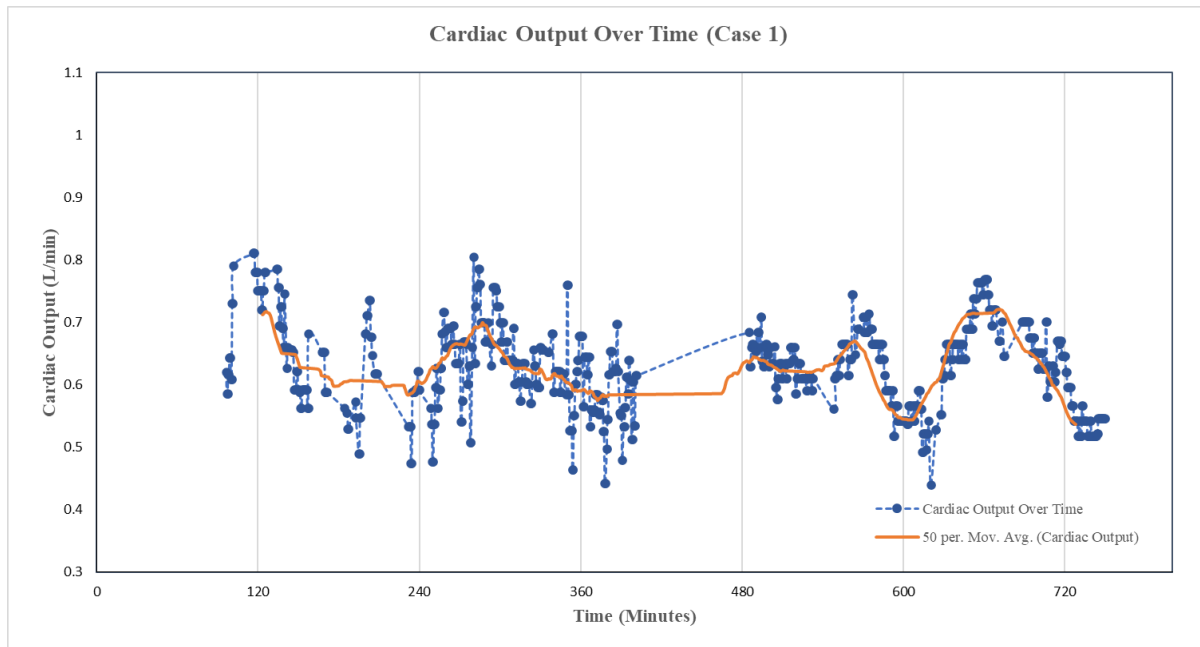


Fig. 18: Mean Cardiac Output over Time (Case 1)

The cardiac output (CO), while slightly lower than reference values, did not vary more than 14% from its mean value throughout the study, which may be considered normal (Fig. 18). The moving average was calculated using a 50-point interval to assess changes in trends of the CO values, and the trendline shows these fluctuations of CO over the recovery period. The reference value of 0.8-1.3 L/min may be slightly too high for this population, as it is an average value for infants aged 0-12 months and not specifically tailored for infants between 0-6 weeks. However, sparse literature exists for this study population; therefore, the variance in cardiac output was considered to be more reflective of cardiac output

assessment than comparison to the reference alone. Similar to cardiac output, the systemic vascular resistance (SVR) values were outside the reference range, which may be a factor of the patient's exact age. Therefore, the overall change in SVR throughout the study was considered a more accurate assessment of the degree of vasoconstriction. For this subject, a lack of a significant increase in the systemic vascular resistance negated suspicion of peripheral vasoconstriction as SVR did not change more than 5% throughout the study. Overall, the general decrease in HR, SVR, central venous pressure (CVP_m) combined with high oxygen saturation values and average CO did not suggest the presence of LCOS or impaired cardiac performance for this patient during the recovery period.

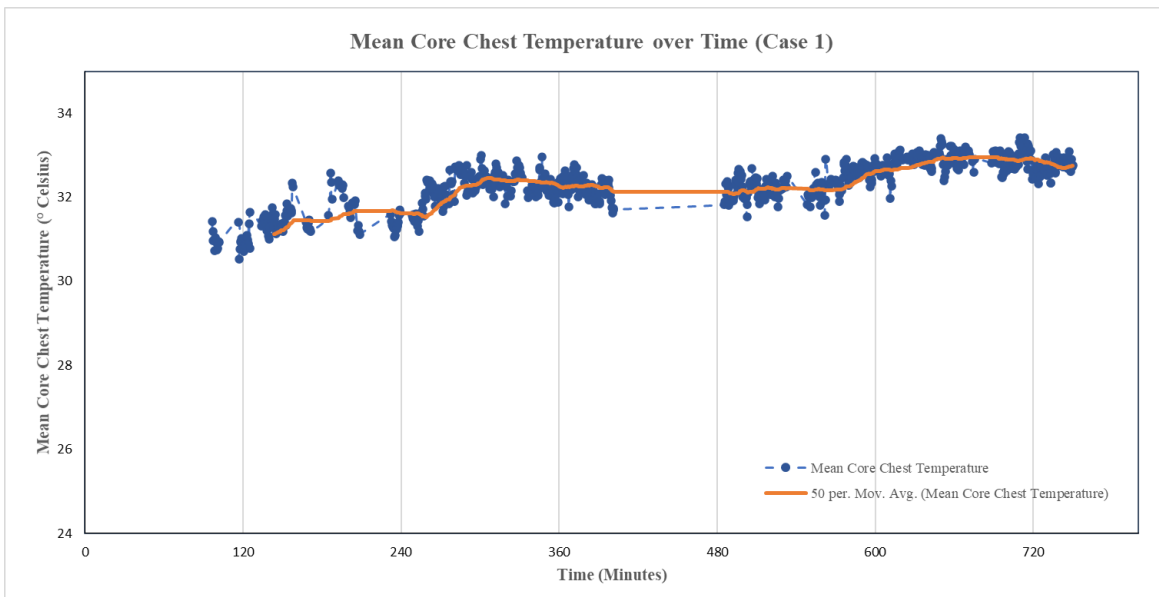


Fig. 19: Mean Core Chest Temperature over Time (Case 1)

The average core temperature of the patient began to normalize over the course of the study, and followed the predicted warm-up pattern as described by Matthews (Fig. 19) [50]. Once the warming state began, the subject's core temperature continuously increased to approximately 33° C in the first 6 hours of the recovery period. As no adverse events were recorded for this subject during the immediate post-operative period, the warming trend matched the expectation for temperature normalization. While the peripheral hand temperatures fluctuated more at the beginning of the study, the peripheral foot temperatures steadily increased from 26 to 28° C in the first 6 hours. The overall increase in peripheral temperature by the 6-hour mark suggested that peripheral perfusion was not restricted for this patient; this finding was supported by the decrease in HR, CVP_m, and SVR hemodynamic values. Interruptions in the sampling of

the peripheral temperature due to the clinical environment prevented further conclusions about the correlation between thermographic and hemodynamic trends beyond the 6-hour mark.

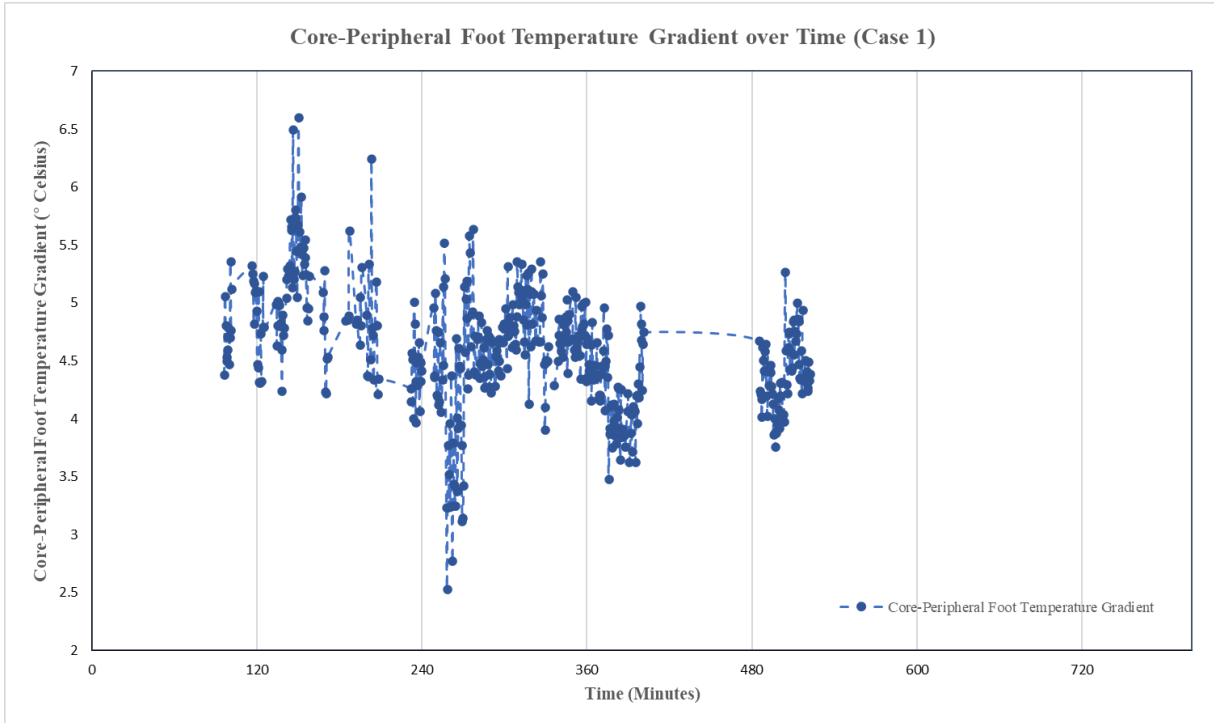


Fig. 20: Core Peripheral Foot Temperature Gradient over Time (Case 1)

The core-peripheral temperature gradient (CPTG) for this subject decreased slightly over time, which indicated that the subject was rewarming as expected and was not manifesting clinical signs of LCOS (Fig. 20). The gradient in this case, was slightly elevated than the reference initially (CPTG \approx 5° C at T = 2 H) and exhibited peak values over 5° C in the first 2.5 hours of the postoperative recovery. However, by the 3-hour mark, the CPTG had decreased, and generally did not exceed 5° C for the rest of the recovery period. The CPTG at the beginning of the study may have been slightly larger than expected but could be related to the hypothermic temperature that the subject was cooled to during surgery. While hypothermia helps provide myocardial protection during CPB, the significant decrease in the patient's body temperature may inflate the CPTG value initially, depending on the degree of hypothermia.

3.2 Pilot Study Analysis

3.2.1 Case 2: Background

In this study, the subject was under 6 months of age, recovering from CHD repair utilizing hypothermic CPB and was reported to have a period of low blood pressure approximately three hours after the start of the study that required pharmaceutical management. Since this case had a documented event related to cardiac performance, it was selected as a suitable candidate for the analysis and evaluation of the subject's thermal profile. Along with the thermal and optical images captured by the same previously described imaging system, the patient's vitals were recorded at hourly intervals with personal identifiers removed. While this protected the patient's privacy, it is important to note that other parameters influencing cardiac performance (such as exact age, body weight, and pharmaceutical administration, etc.) were unavailable and could not be directly evaluated in this case. However, despite this limitation, some trends could be observed at the reported event time that provided valuable insight into the thermal profile during impaired recovery in the postoperative period.

A note given by the attending clinician for this case study described a drop in blood pressure at hour 3 of the study and that some supportive medication was given at that time to help improve the patient's cardiac output. This major adverse event provides an illustrative abnormal recovery profile for consideration to help guide ongoing and future improvements of the quantification protocol. Given the documented insights from the clinicians for this subject, most of the quantitative analysis focuses on the initial twelve-hour time period immediately after surgery to document the recovery profile. The overall goal of the analysis of this study is to provide insight into a recorded adverse event potentially caused by LCOS and to document the patient's recovery profile for additional study comparisons.

3.2.2 Discussion

Table 4: Observed and Calculated Hemodynamic Monitoring Values (Case 2)

Observed and Calculated Hemodynamic Monitoring Values (Case 2)								
Hour	Oxygen Saturation (SpO2) (%)	Systolic Pressure (mmHg)	Diastolic Pressure (mmHg)	MAP (mmHg)	HR (BPM)	Central Venous Pressure (CVPm) (mmHg)	Cardiac Output (L/min)	Systemic Vascular Resistance (SVR) (dynes/s/cm ²)
0	94	82	47	51	125	10	0.89	3748.6
1	94	77	41	53	111	10	0.80	4304.3
2	95	76	42	54	110	9	0.75	4812.8
3	95	63	38	46	104	11	0.52	5384.6
4	95	62	39	46	140	12	0.64	4223.6
5	96	72	42	51	140	12	0.84	3714.3
6	97	73	43	52	140	11	0.84	3904.8
7	97	69	42	50	140	11	0.76	4127.0
8	98	74	45	54	140	12	0.81	4137.9
10	97	71	43	52	142	12	0.80	4024.1
11	97	81	46	58	140	10	0.98	3918.4
12	98	75	43	54	140	10	0.90	3928.6
13	100	77	44	56	140	8	0.92	4155.8
14	98	84	48	62	140	11	1.01	4047.6
15	99	86	58	64	140	11	0.78	5408.2
16	96	79	49	62	140	6	0.84	5333.3
17	96	72	45	56	140	8	0.76	5079.4
18	99	71	45	56	140	9	0.73	5164.8

Table 4 describes the measured and calculated hemodynamic values that were monitored in this case study, with hemodynamic vitals at hour 3 highlighted for illustration of abnormal trends in the recovery profile. Unfortunately, since the obtained vital data set was only recorded per hour, minute-by-minute analysis of the change in hemodynamic values could not be completed. However, the quantification of the thermal profile helped provide more information about the patient’s cardiovascular status, as it demonstrated a marked change in temperature values before the reported event (see Chapter I, subsection 1.2.7).

Table 5: Hemodynamic Values Comparison at T = 3H (Case 2)

Hemodynamic Values Comparison at T = 3 H (Case 2)

Parameter	Mean Value, T=0 to T=18 H	Mean Value, T=3 H	Percent Difference
Oxygen Saturation (SpO2) (%)	96.7	95	-1.78
Systolic Pressure (mmHg)	74.7	63	-15.63
Diastolic Pressure (mmHg)	44.4	38	-14.50
MAP (mmHg)	54.3	46	-15.30
HR (BPM)	134	104	-22.39
Central Venous Pressure (CVPm) (mmHg)	10.2	11	8.20
Cardiac Output (L/min)	0.81	0.52	35.74
Systemic Vascular Resistance (dynes/s/cm ²)	4234.3	5384.6	22.04

At hour 3, the patient exhibited a marked decrease in both systolic and diastolic blood pressure, mean arterial pressure, heart rate, and cardiac output. Table 5 examines these differences in detail and provides more context for how these values differed from the patient’s average hemodynamic values throughout the study. Strikingly, the CO was 35% lower than its mean value by the time of the reported event. This decrease in CO was greater than the decrease in CO observed in Case 1, which was no more than 30% decreased throughout their recovery. The greater decrease in CO in Case 2 marked a potential difference between normal and abnormal recovery profiles. However, the reduction in the patient’s heart rate (by over 20% from its average) did not meet the tachycardic criteria that is associated with LCOS. Additional hemodynamic assessment revealed that the systolic, diastolic, and mean arterial pressures were each about 15% lower than their mean value at the time of the reported event, which indicated a decrease in the patient’s stroke volume. The decrease in CO and HR at the same time point provided further evidence

of this observation. The SVR was increased by approximately 22% during the reported event and indicated a potential rise in peripheral vasoconstriction. The CVP_m was also elevated during this time point and was at the top end of the reference range and reflected the decrease in CO. The decrease in blood pressure and heart rate, coupled with the rise in SVR and CVP_m, may be considered an early sign of hypovolemic shock and provided rationale for the clinical decision to administer medication and fluids at this time point. Overall, these findings suggested that the patient was exhibiting signs of impaired cardiac function and potentially, LCOS before the clinical intervention [19, 20].

Table 6: Normal Reference Hemodynamic Values for Infants

Normal Reference Hemodynamic Values for Infants		
Parameter	Reference Values	Source
Oxygen Saturation (SpO ₂) (%)	>72%	Meskhishvilli [52]
Systolic Pressure (mmHg)	74-100	Meskhishvilli [52]
Diastolic Pressure (mmHg)	50-70	Boville [27]
MAP (mmHg)	> 55 mmHg	Joffe [24]
HR (BPM)	120-160	Boville [27]
Central Venous Pressure (CVP _m) (mmHg)	11.25 mmHg	Song [8]
Cardiac Output (L/min)	0.8-1.3	Boville [27]
Systemic Vascular Resistance (SVR) (dynes*s/cm ²)	2800-4000	Boville [27]
Core Temperature (° Celsius)	34-36°	Matthews [50]
Peripheral Temperature (° Celsius)	> 29° by 6 h	Gupta [47]
Core-Peripheral Temperature Gradient (° Celsius)	< 5	Song [8]

When the hemodynamic values recorded for Case 2 were compared to the reference values, more abnormal trends in the vital values were deciphered (Table 6). At the 3-hour time point, the diastolic blood pressure in Case 2 (38 mmHg) had decreased below the reference range of 50-70 mmHg; this value was also considerably lower than the diastolic blood pressure recorded for Case 1 at the same time point (~50 mmHg). The MAP in Case 2 (46 mmHg) had also decreased below its reference value of 55 mmHg by the 3-hour mark, which was much lower than the MAP recorded for Case 1 (56 mmHg) at the same point. Additionally, the HR in Case 2 (104 BPM) was much lower than the reference range and the HR measured in Case 1 (148 BPM) at the 3-hour mark of recovery. Overall, the comparison of hemodynamic values to the reference values and between Case 1 and Case 2 highlighted unique differences in the recovery profile of both subjects after surgery.

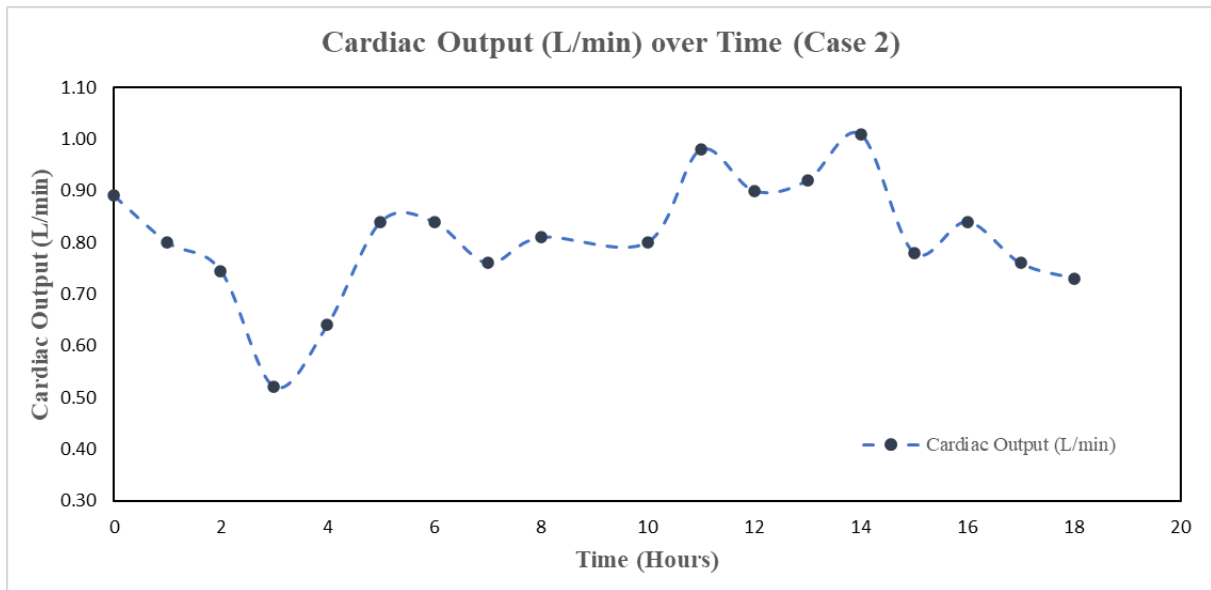


Fig. 21: Cardiac Output (L/min) over Time (Case 2)

Cardiac output was also different between both cases at the time of the reported event in Case 2. At the 3-hour mark, a sharp decrease in CO was observed for Case 2, and its value was 35% lower than its average value and CO measured at the same time point for Case 1 (Fig. 21). However, the gap between the recorded vital measurements prevented a more concrete identification of decreasing CO in Case 2. Analysis of the thermographic trends for this patient was therefore considered a high priority to decipher if significant changes in temperature preceded the dramatic change in hemodynamic values observed at the 3-hour mark.

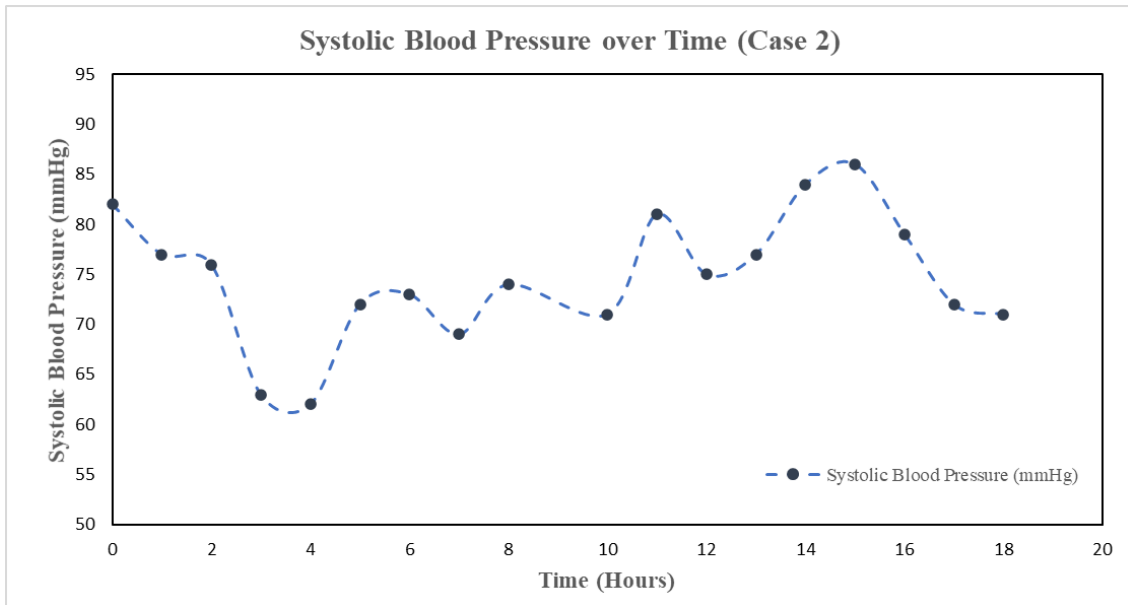


Fig. 22: Systolic Blood Pressure over Time (Case 2)

A similar sharp and sudden decrease was observed in the SBP measurements for Case 2 at the time of the reported event, which was documented as part of the clinician’s decision to intervene with medication (Fig. 22). After the intervention, the SBP increased to clinically acceptable values, and did not exhibit another large decrease from average values.

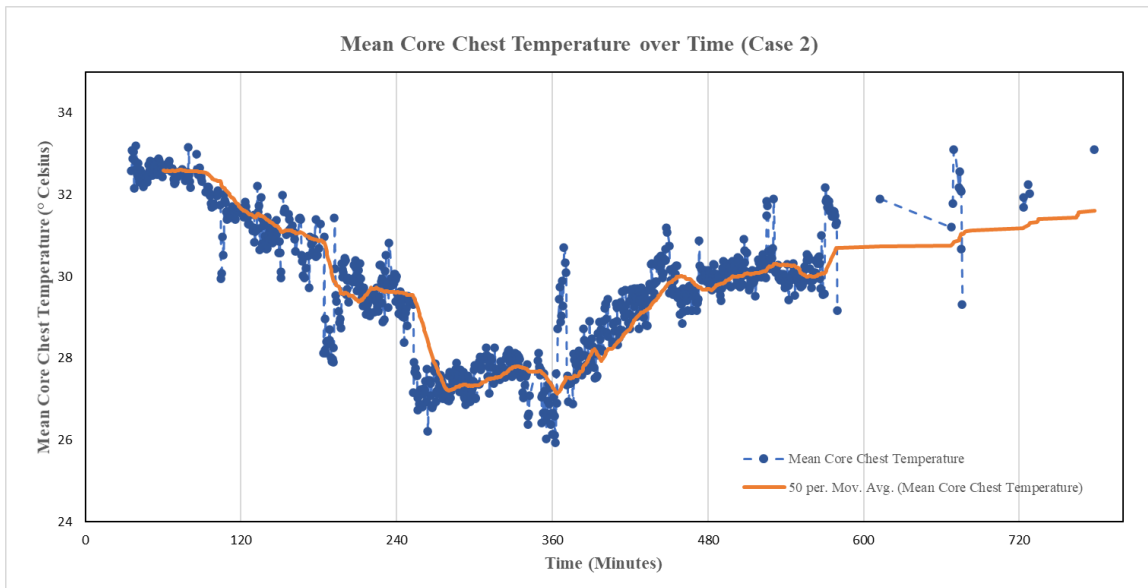


Fig. 23: Mean Core Chest Temperature over Time (Case 2)

In the second hour of the study, the core chest temperature in Case 2 steadily decreased from approximately 32.5° C to 31.5° C, which was below the ideal reference temperature range (32-34° C) (Fig. 23). The core temperature continued to decrease over the next hour until the time of the reported event at the 3-hour time point, which is not expected in normal warm-up patterns after surgery. After the clinical intervention, the core temperature continued to decrease until the 6-hour time point, where the core temperature was as low as 27° C. The decrease in core temperature was in stark contrast with Case 1, which continuously increased throughout the recovery period at higher temperature values (Fig. 19). The observed change in the core temperature by the 2-hour time point in Case 2 and the lack of normalized core temperature by the 6-hour mark highlighted another potential difference between normal and abnormal recovery profiles and seemed to provide more context for the sudden change in hemodynamic values by the 3-hour time point.

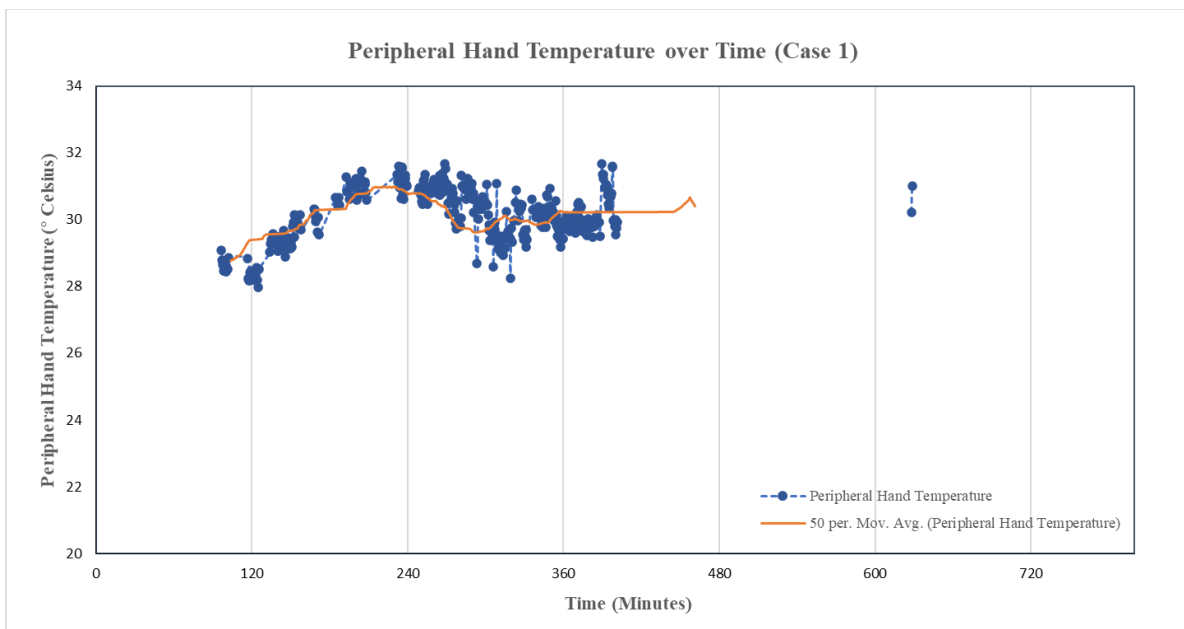


Fig. 24: Peripheral Hand Temperature Over Time (Case 1)

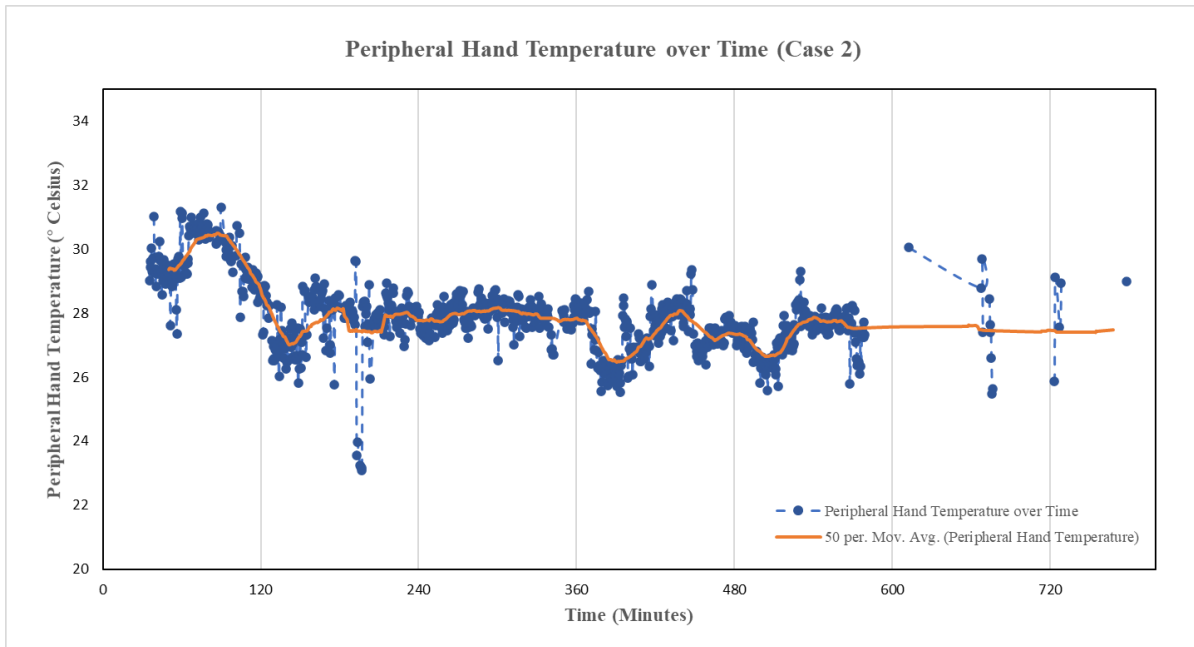


Fig. 25: Peripheral Hand Temperature Over Time (Case 2)

Differences in other thermal profiles between Case 1 and Case 2 provided further examples of normal and abnormal recovery trends. While the thermal profile for Case 1 was incomplete due to obscurement of the peripheral limbs during the clinical protocol, it still provided a basis for comparison of the 2- to 3-hour time points to that of Case 2. In Case 1, the peripheral hand temperature increased to approximately 30.5° C by the 3-hour time point before plateauing during the 3–6-hour period (Fig. 24). While there was some variation in the trendline, the peripheral hand temperature was higher overall than documented in Case 2 (Fig. 25). Despite a slight increase in hand temperature in the first hour of the Case 2, there was a noticeable decline in temperature between the first hour and second hour, before the temperature plateaued to approximately 28° C between the 4th and 6th hour time point. The plateau may have been influenced by the placement of the arm on top of a heated blanket and may explain why peripheral temperature did not decrease along with the core chest temperature. Notably, the decline in peripheral hand temperature in the first 2 hours of the study preceded the change in core temperature in Case 2 and was also larger in magnitude. This decrease supported the suspicion of LCOS in the second patient, as low peripheral temperature (<29° C) indicates peripheral vasoconstriction [69].

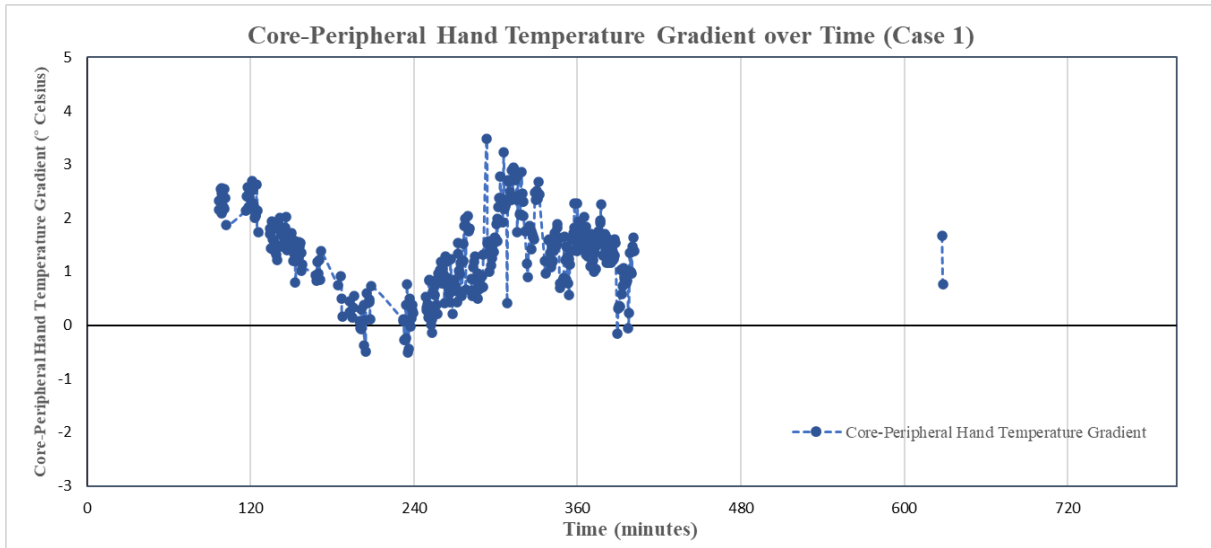


Fig. 26: Core-Peripheral Hand Temperature Gradient Over Time (Case 1)

The core-peripheral hand temperature gradient highlighted additional differences in the recovery profile between Case 1 and Case 2. The gradient was calculated by subtracting the peripheral hand temperature from the core temperature values, as described in Chapter I (subsection 1.2.7). Comparison between the core-peripheral foot temperature gradients in both cases was not feasible due to the lack of exposed limbs during the clinical protocol in Case 2. Case 1 also exhibited some incompleteness in the core-peripheral hand temperature gradient, but it did provide some data for comparison between 2-6 hours. In Case 1, the CPTG continuously decreased between the 2nd and 3rd hour time point before it increased between the 3rd and 5th hour time point (Fig. 26) [70]. However, by the 6-hour time point, the CPTG normalized to approximately 2° C, which is expected in normal recovery. The fluctuation in the CPTG requires further investigation to determine its cause and see if the fluctuations are consistent with normal recovery profiles. Overall, the CPTG did not exceed the reference range for LCOS, and its graphical trend supported the hemodynamic analysis that concluded LCOS was not present in this patient.

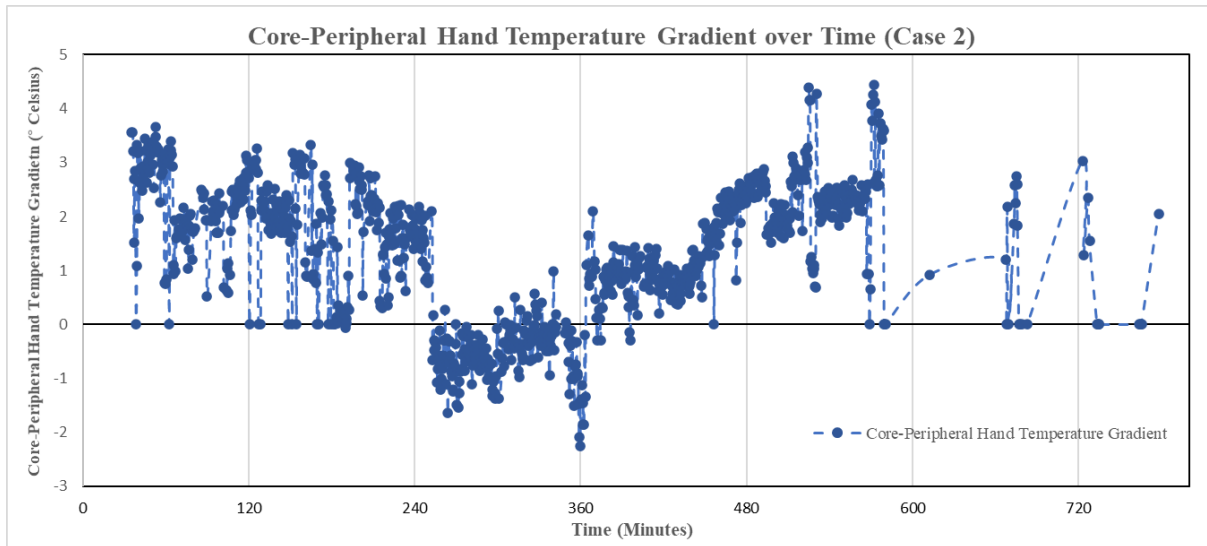


Fig. 27: Core-Peripheral Hand Temperature Gradient over Time (Case 2)

In Case 2, the CPTG was approximately 1-2° C higher than in Case 1 in the first two hours of the study (Fig. 27). However, at the four-hour mark, the gradient sharply decreased. The change in trend was caused by the continuous decrease in the core temperature for this patient and the plateau of the peripheral temperature, which resulted in a decreasing difference between the core and peripheral temperatures. The peripheral temperature was abnormally elevated with respect to core temperature between the 4th and 6th hour time points, but that was likely because of the placement of the arm on top of a heated blanket during that time period. Although the CPTG did not specifically indicate that LCOS may be present by the time of the reported event, the presence of a depressed core temperature during the recovery period may provide the clinical basis for LCOS diagnosis.

While the sample size is too small to provide reliable statistical significance, the presented analysis provides a preliminary insight into recovery profiles in this population. Even with limited comparison, differences in the thermal trends between Case 1 and Case 2 could be observed, and some thermal observations in Case 2 preceded significant changes in the monitored hemodynamic values. Overall, the analysis served to establish a thermal quantification protocol in a critical care environment that could facilitate the identification of thermographic trends in an underreported population.

CHAPTER IV

CONCLUSIONS AND FUTURE WORK

1.1 Conclusions

Overall, the body of work presented satisfied the two primary objectives of establishing a thermal quantification protocol and initial analysis of eligible case studies. The development of the thermal quantification protocol took a significant amount of dedication to ensure that it was dynamic enough to analyze multiple different types of case studies, which is particularly challenging in an acute care clinical environment. The health, safety and comfort of the patients is the ultimate priority when conducting these clinical studies; therefore, interruptions in study observations and incomplete data sets are expected and motivate the need for additional case analysis. As part of my work on this project, I developed all three MATLAB scripts for the image quality screening, registration, segmentation, and analysis. I also generated extensive documentation to ensure that the thermographic analysis stays consistent across operators and in compliance with IRB standards. The initial analysis of the two case studies shows promise in monitoring thermographic trends in a fragile pediatric population, and differences observed between the “normal” and “abnormal” recovery profiles provides motivation for future case analysis.

2.1 Future Work

In the future, more case analysis will need to be completed to verify observed thermographic trends in the recovery profile of pediatric cardiac surgery patients and to continue the movement of the thermal quantification protocol towards complete autonomy. The evaluation of SvO₂ with thermographic trends must also be incorporated in the future work and recording of that value must be explicitly incorporated in the protocol. Eventually, the overall goal of the system is to be able to run independently in a pediatric cardiac care unit and have thermographic analysis calculated instantaneously. Potentially, if enough thermographic trends are observed, and their correlation to hemodynamic values statistically verified, the system will be able to provide an early warning to clinicians that low cardiac output syndrome (LCOS) may be developing in the patient.

As part of my commitment to develop the thermographic imaging system towards future goals, I have begun work on a proprietary piece of software that performs the thermographic analysis in MATLAB,

called the “Cycle Tracker”. The aim of the software is to calculate relevant thermographic and hemodynamic values, compare them, and output relevant pieces of information on a “warning card” to the cardiac care team. The software focuses on tracking altered temperature values in each region of interest and performing statistical evaluation to dynamically determine if temperatures in the region are increasing, decreasing, and/or are associated with significant changes in hemodynamic values.

A “cycle” is considered when the temperature in a defined region is significantly different than its baseline temperature, whether it is higher or lower than the average value. If there is not an injection in the nearby range and the change persists for a minute or longer, the elevated or depressed portion is considered a “cycle”. The frequency of these cycles is evaluated along with time of day, long lasting effects of medications, vital values, and NIRS values. Statistically significant changes in these values add weight to the cycle grade, which suggests that the cycles are associated with development of early onset LCOS symptoms. Weight is added to the cycle grade via a symbol system. A significant change in temperature adds a “+” to the cycle score, and a significant change in vital values or other measurements adds an additional “+” to the score. Cycles have a maximum score of two symbols, with a minimum of no symbols further defining the score range. Cycles with more weight are considered better predictors of LCOS symptoms rather than cycles with less weight; lighter cycles are not associated with as many key changes and may be reflections of medication effects or sleep cycle rhythms.

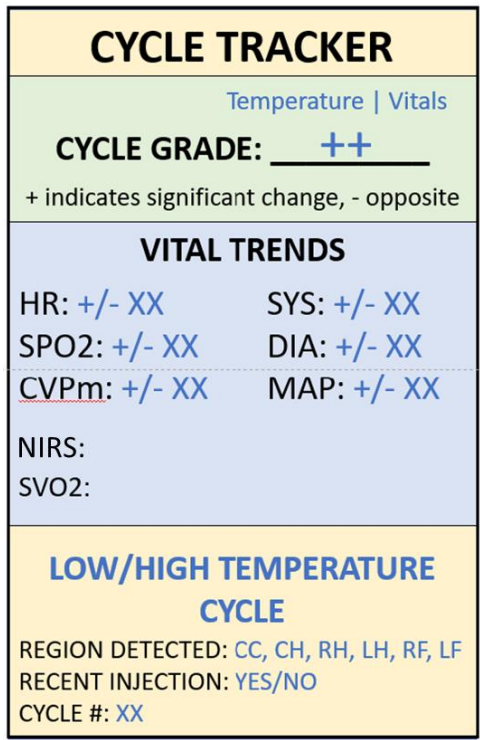


Fig. 28: Cycle Tracker Report Card

A provisional piece of software has been written that outputs the conclusions of the analysis methods in a simple scorecard to provide the clinical care team with a succinct warning and displays additional considerations in a format that is easily understandable. This method allows the clinical care staff to make informed, rapid decisions as the score card provides the key changed values in an aim to reduce time deciphering the trends individually and improve early intervention techniques (Fig. 28). Immediately after the cycle grade, the vital trends are reported along with any key statistical changes, such as “+20 BPM”, indicating that the heart rate has been significantly elevated than the baseline by an increase of 20 BPM. Any significant changes in the NIRS or SvO₂ values are also reported; however, these changes are better represented by simple “significantly elevated” or “significantly decreased”, a decision informed by the clinical care team’s utilization of these particular measurement techniques. Lastly, the score card provides the clinicians with more information about the thermographic trends, including whether the temperature is elevated or depressed, in which region this change was identified, if a recent injection should be considered, and the cycle number (tracked from the beginning of monitoring). This score card may be additionally output to the figures generated in the image registration and segmentation procedure and saved in an .mp4 format for future review.

Additionally, future work may include the implementation of artificial intelligence (AI) and deep learning methods to improve the speed of the thermal quantification protocol. In particular, AI methods should be used to automatically screen obtained images for quality, register the optical and thermal images together, and to segment the primary regions of interest from the co-registered images. This implementation would greatly improve the efficiency of case analysis and would enhance user capability to process more sets of data over time.

REFERENCES

- [1] J. I. Hoffman, "The global burden of congenital heart disease," *Cardiovasc. J. Afr.*, vol. 24, no. 4, pp. 141–145, Jun. 2013, doi: 10.5830/CVJA-2013-028.
- [2] Y. Liu *et al.*, "Global birth prevalence of congenital heart defects 1970–2017: updated systematic review and meta-analysis of 260 studies," *Int. J. Epidemiol.*, vol. 48, no. 2, pp. 455–463, Apr. 2019, doi: 10.1093/ije/dyz009.
- [3] I. of M. (US) C. on S. S. C. D. Criteria, *Congenital Heart Disease*. National Academies Press (US), 2010. Accessed: Jul. 09, 2021. [Online]. Available: <https://www.ncbi.nlm.nih.gov/books/NBK209965/>
- [4] D. Huisenga, S. La Bastide-Van Gemert, A. Van Bergen, J. Sweeney, and M. Hadders-Algra, "Developmental outcomes after early surgery for complex congenital heart disease: a systematic review and meta-analysis," *Dev. Med. Child Neurol.*, vol. 63, no. 1, pp. 29–46, Jan. 2021, doi: 10.1111/dmcn.14512.
- [5] S. Abqari, A. Gupta, T. Shahab, M. Rabbani, S. M. Ali, and U. Firdaus, "Profile and risk factors for congenital heart defects: A study in a tertiary care hospital," *Ann. Pediatr. Cardiol.*, vol. 9, no. 3, pp. 216–221, 2016, doi: 10.4103/0974-2069.189119.
- [6] K. A. Holst, S. M. Said, T. J. Nelson, B. C. Cannon, and J. A. Dearani, "Current Interventional and Surgical Management of Congenital Heart Disease," *Circ. Res.*, vol. 120, no. 6, pp. 1027–1044, Mar. 2017, doi: 10.1161/CIRCRESAHA.117.309186.
- [7] H. K. Chandler and R. Kirsch, "Management of the Low Cardiac Output Syndrome Following Surgery for Congenital Heart Disease," *Curr. Cardiol. Rev.*, vol. 12, no. 2, pp. 107–111, May 2016, doi: 10.2174/1573403X12666151119164647.
- [8] B. Song, H. Dang, and R. Dong, "Analysis of risk factors of low cardiac output syndrome after congenital heart disease operation: what can we do," *J. Cardiothorac. Surg.*, vol. 16, p. 135, May 2021, doi: 10.1186/s13019-021-01518-7.
- [9] G. V. Parr, E. H. Blackstone, and J. W. Kirklin, "Cardiac performance and mortality early after intracardiac surgery in infants and young children.," *Circulation*, vol. 51, no. 5, pp. 867–874, May 1975, doi: 10.1161/01.CIR.51.5.867.
- [10] M. J. Nordness, A. C. Westrick, H. Chen, and M. A. Clay, "Identification of Low Cardiac Output Syndrome at the Bedside: A Pediatric Cardiac Intensive Care Unit Survey | Critical Care Nurse | American Association of Critical-Care Nurses," *Crit. Care Nurse*, vol. 39, no. 2, pp. E1–E7, Apr. 2019, doi: <https://doi.org/10.4037/ccn2019794>.
- [11] T. Schub, O. Oji, D. Strayer, T.-L. Spears, and D. Pravikoff, "Nursing Quick Lesson: Low Cardiac Output Syndrome." Nursing Reference Center Plus, Mar. 26, 2021. [Online]. Available: <https://www.google.com/url?sa=t&rct=j&q=&esrc=s&source=web&cd=&cad=rja&uact=8&ved=2ahUKEwj6ovTei5f0AhXzTDABHWT4BzkQFnoECAQQAQ&url=https%3A%2F%2Fwww.ebsco.com%2Fsites%2Fg%2Ffiles%2Fnabnos191%2Ffiles%2Facquiadam-assets%2FNursing-Reference-Center-Plus-Quick-Lesson-Low-Cardiac-Output-Syndrome.pdf&usg=AOvVaw0zJAS4E-cCWYnWj2hEAQP>
- [12] L. E. Conrad, E. M. Mary, L. W. Eric, and M. C. John, "Pathophysiology of Post-Operative Low Cardiac Output Syndrome," *Curr. Vasc. Pharmacol.*, vol. 14, no. 1, pp. 14–23, Dec. 2015.
- [13] X. Du *et al.*, "Risk factors for low cardiac output syndrome in children with congenital heart disease undergoing cardiac surgery: a retrospective cohort study," *BMC Pediatr.*, vol. 20, no. 1, p. 87, Feb. 2020, doi: 10.1186/s12887-020-1972-y.
- [14] T. M. Hoffman *et al.*, "Efficacy and safety of milrinone in preventing low cardiac output syndrome in infants and children after corrective surgery for congenital heart disease," *Circulation*, vol. 107, no. 7, pp. 996–1002, Feb. 2003, doi: 10.1161/01.cir.0000051365.81920.28.

- [15] B. Jones, M. Hayden, J. F. Fraser, and E. Janes, “Low cardiac output syndrome in children - ScienceDirect,” *Curr. Anaesth. Crit. Care*, vol. 16, no. 6, pp. 347–358, 2005, doi: <https://doi.org/10.1016/j.cacc.2006.02.011>.
- [16] K. P. Ulate, O. Yanay, H. Jeffries, H. Baden, J. L. Di Gennaro, and J. Zimmerman, “An Elevated Low Cardiac Output Syndrome Score Is Associated With Morbidity in Infants After Congenital Heart Surgery,” *Pediatr. Crit. Care Med. J. Soc. Crit. Care Med. World Fed. Pediatr. Intensive Crit. Care Soc.*, vol. 18, no. 1, pp. 26–33, Jan. 2017, doi: 10.1097/PCC.0000000000000979.
- [17] G. Wernovsky *et al.*, “Postoperative Course and Hemodynamic Profile After the Arterial Switch Operation in Neonates and Infants,” *Circulation*, vol. 92, no. 8, pp. 2226–2235, Oct. 1995, doi: 10.1161/01.CIR.92.8.2226.
- [18] J. Kobe, N. Mishra, V. K. Arya, W. Al-Moustadi, W. Nates, and B. Kumar, “Cardiac Output Monitoring: Technology and Choice,” *Ann. Card. Anaesth.*, vol. 22, no. 1, pp. 6–17, 2019, doi: 10.4103/aca.ACA_41_18.
- [19] L. Massé and M. Antonacci, “Low Cardiac Output Syndrome: Identification and Management,” *Crit. Care Nurs. Clin. North Am.*, vol. 17, no. 4, pp. 375–383, Dec. 2005, doi: 10.1016/j.ccell.2005.07.005.
- [20] H. Krishnan, M. R. Fine-Goulden, S. Raman, and A. Deep, *Challenging Concepts in Pediatric Critical Care: Cases with Expert Commentary*. Oxford University Press, 2020. [Online]. Available: <https://oxfordmedicine.com/view/10.1093/med/9780198794592.001.0001/med-9780198794592>
- [21] J. Koenig, L. K. Hill, D. P. Williams, and J. F. Thayer, “ESTIMATING CARDIAC OUTPUT FROM BLOOD PRESSURE AND HEART RATE: THE LILJESTRAND & ZANDER FORMULA,” *Biomed. Sci. Instrum.*, vol. 51, pp. 85–90, 2015.
- [22] N. Patel, J. Durland, and A. N. Makaryus, “Physiology, Cardiac Index,” in *StatPearls*, Treasure Island (FL): StatPearls Publishing, 2021. Accessed: Nov. 14, 2021. [Online]. Available: <http://www.ncbi.nlm.nih.gov/books/NBK539905/>
- [23] A. Cavigelli-Brunner *et al.*, “Prevention of Low Cardiac Output Syndrome After Pediatric Cardiac Surgery: A Double-Blind Randomized Clinical Pilot Study Comparing Dobutamine and Milrinone,” *Pediatr. Crit. Care Med.*, vol. 19, no. 7, Art. no. 7, Mar. 2018, doi: 10.1097/PCC.0000000000001533.
- [24] A. R. Joffe, C. M. T. Robertson, A. Nettel-Aguirre, I. M. Rebeyka, and R. S. Sauve, “Mortality after neonatal cardiac surgery: Prediction from mean arterial pressure after rewarming in the operating room,” *J. Thorac. Cardiovasc. Surg.*, vol. 134, no. 2, pp. 311–318, Aug. 2007, doi: 10.1016/j.jtcvs.2007.02.001.
- [25] B.-H. Victor, K. Georgios, D. M. James, and J. del N. Pedro, “Cellular and Molecular Mechanisms of Low Cardiac Output Syndrome after Pediatric Cardiac Surgery,” *Curr. Vasc. Pharmacol.*, vol. 14, no. 1, pp. 5–13, Dec. 2015.
- [26] A. C. Celotto, L. G. Ferreira, V. K. Capellini, A. A. S. Albuquerque, A. J. Rodrigues, and P. R. B. Evora, “Acute but not chronic metabolic acidosis potentiates the acetylcholine-induced reduction in blood pressure: an endothelium-dependent effect,” *Braz. J. Med. Biol. Res.*, vol. 49, no. 2, p. e5007, Dec. 2015, doi: 10.1590/1414-431X20155007.
- [27] B. Boville and L. C. Young, *Quick Guide to Pediatric Cardiopulmonary Care*. Edwards LifeSciences, 2015.
- [28] P. Shah and M. A. Louis, “Physiology, Central Venous Pressure,” in *StatPearls*, Treasure Island (FL): StatPearls Publishing, 2021. Accessed: Nov. 25, 2021. [Online]. Available: <http://www.ncbi.nlm.nih.gov/books/NBK519493/>
- [29] L. Su *et al.*, “Central Venous Pressure (CVP) Reduction Associated With Higher Cardiac Output (CO) Favors Good Prognosis of Circulatory Shock: A Single-Center, Retrospective Cohort Study,” *Front. Med.*, vol. 6, p. 216, 2019, doi: 10.3389/fmed.2019.00216.
- [30] L. E. Issac, S. Fugar, N. Yamani, and B. Mohamedali, “Acute Heart Failure Exacerbation with Cardiogenic Shock and Elevated Systemic Vascular Resistance Treated with a Combination of

- Nicardipine and Dobutamine Therapy,” *Case Rep. Cardiol.*, vol. 2017, p. 7329213, 2017, doi: 10.1155/2017/7329213.
- [31] C. Vahdatpour, D. Collins, and S. Goldberg, “Cardiogenic Shock,” *J. Am. Heart Assoc. Cardiovasc. Cerebrovasc. Dis.*, vol. 8, no. 8, p. e011991, Apr. 2019, doi: 10.1161/JAHA.119.011991.
- [32] D. de Souza, G. M. McDaniel, and V. C. Baum, “CHAPTER 4 - Cardiovascular Physiology,” in *Smith’s Anesthesia for Infants and Children (Eighth Edition)*, P. J. Davis, F. P. Cladis, and E. K. Motoyama, Eds. Philadelphia: Mosby, 2011, pp. 80–115. doi: 10.1016/B978-0-323-06612-9.00004-3.
- [33] J. Mallat *et al.*, “Ratios of central venous-to-arterial carbon dioxide content or tension to arteriovenous oxygen content are better markers of global anaerobic metabolism than lactate in septic shock patients,” *Ann. Intensive Care*, vol. 6, p. 10, Feb. 2016, doi: 10.1186/s13613-016-0110-3.
- [34] S. Chetana Shanmukhappa and S. Lokeshwaran, “Venous Oxygen Saturation,” in *StatPearls*, Treasure Island (FL): StatPearls Publishing, 2021. Accessed: Dec. 01, 2021. [Online]. Available: <http://www.ncbi.nlm.nih.gov/books/NBK564395/>
- [35] P. van Beest, G. Wietasch, T. Scheeren, P. Spronk, and M. Kuiper, “Clinical review: use of venous oxygen saturations as a goal - a yet unfinished puzzle,” *Crit. Care*, vol. 15, no. 5, p. 232, 2011, doi: 10.1186/cc10351.
- [36] L. A. Rhodes, W. C. Erwin, S. Borasino, D. C. Cleveland, and J. A. Alten, “Central venous to arterial carbon dioxide difference monitoring after cardiac surgery in infants and neonates,” *Pediatr. Crit. Care Med. J. Soc. Crit. Care Med. World Fed. Pediatr. Intensive Crit. Care Soc.*, vol. 18, no. 3, pp. 228–233, Mar. 2017, doi: 10.1097/PCC.0000000000001085.
- [37] A. Yadlapati, T. Grogan, D. Elashoff, and R. B. Kelly, “Correlation of a Novel Noninvasive Tissue Oxygen Saturation Monitor to Serum Central Venous Oxygen Saturation in Pediatric Patients with Postoperative Congenital Cyanotic Heart Disease,” *J. Extra. Corpor. Technol.*, vol. 45, no. 1, pp. 40–45, Mar. 2013.
- [38] J. K. Kirklin, E. H. Blackstone, J. W. Kirklin, R. McKay, A. D. Pacifico, and L. M. Barger, “Intracardiac surgery in infants under age 3 months: predictors of postoperative in-hospital cardiac death,” *Am. J. Cardiol.*, vol. 48, no. 3, pp. 507–512, Sep. 1981, doi: 10.1016/0002-9149(81)90080-1.
- [39] P. Cowled and R. Fitridge, “Pathophysiology of Reperfusion Injury,” in *Mechanisms of Vascular Disease: A Reference Book for Vascular Specialists*, R. Fitridge and M. Thompson, Eds. Adelaide (AU): University of Adelaide Press, 2011. Accessed: Nov. 25, 2021. [Online]. Available: <http://www.ncbi.nlm.nih.gov/books/NBK534267/>
- [40] C. B. Overgaard and V. Džavík, “Inotropes and Vasopressors,” *Circulation*, vol. 118, no. 10, pp. 1047–1056, Sep. 2008, doi: 10.1161/CIRCULATIONAHA.107.728840.
- [41] S. M. Tibby, M. Hatherill, and I. A. Murdoch, “Capillary refill and core-peripheral temperature gap as indicators of haemodynamic status in paediatric intensive care patients,” *Arch. Dis. Child.*, vol. 80, no. 2, p. 163, Feb. 1999, doi: <http://dx.doi.org/10.1136/adc.80.2.163>.
- [42] R. L. Hickok, M. C. Spaeder, J. T. Berger, J. J. Schuette, and D. Klugman, “Postoperative Abdominal NIRS Values Predict Low Cardiac Output Syndrome in Neonates,” *World J. Pediatr. Congenit. Heart Surg.*, vol. 7, no. 2, pp. 180–184, Mar. 2016, doi: 10.1177/2150135115618939.
- [43] U. S. Bhalala *et al.*, “Change in regional (somatic) near-infrared spectroscopy is not a useful indicator of clinically detectable low cardiac output in children after surgery for congenital heart defects,” *Pediatr. Crit. Care Med. J. Soc. Crit. Care Med. World Fed. Pediatr. Intensive Crit. Care Soc.*, vol. 13, no. 5, pp. 529–534, Sep. 2012, doi: 10.1097/PCC.0b013e3182389531.
- [44] B. M. Schey, D. Y. Williams, and T. Bucknall, “Skin temperature and core-peripheral temperature gradient as markers of hemodynamic status in critically ill patients: a review,” *Heart Lung J. Crit. Care*, vol. 39, no. 1, pp. 27–40, Feb. 2010, doi: 10.1016/j.hrtlng.2009.04.002.
- [45] A. Aynsley-Green and D. Pickering, “Use of central and peripheral temperature measurements in care of the critically ill child,” *Arch. Dis. Child.*, vol. 49, no. 6, pp. 477–481, Jun. 1974.

- [46] A. Lima and J. Bakker, “Noninvasive monitoring of peripheral perfusion,” *Intensive Care Med.*, vol. 31, no. 10, pp. 1316–1326, Oct. 2005, doi: 10.1007/s00134-005-2790-2.
- [47] A. Gupta, J. Puliyeel, B. Garg, and P. Upadhyay, “Mean core to peripheral temperature difference and mean lactate levels in first 6 hours of hospitalisation as two indicators of prognosis: an observational cohort study,” *BMC Pediatr.*, vol. 20, no. 1, p. 515, Nov. 2020, doi: 10.1186/s12887-020-02418-w.
- [48] H. R. Joly and M. H. Weil, “Temperature of the Great Toe as an Indication of the Severity of Shock,” *Circulation*, vol. 39, no. 1, pp. 131–138, Jan. 1969, doi: 10.1161/01.CIR.39.1.131.
- [49] I. A. Murdoch, S. A. Qureshi, A. Mitchell, and I. C. Huggon, “Core-peripheral temperature gradient in children: does it reflect clinically important changes in circulatory haemodynamics?,” *Acta Paediatr. Oslo Nor.* 1992, vol. 82, no. 9, pp. 773–776, Sep. 1993, doi: 10.1111/j.1651-2227.1993.tb12556.x.
- [50] H. R. Matthews, J. B. Meade, and C. C. Evans, “Peripheral vasoconstriction after open-heart surgery,” *Thorax*, vol. 29, no. 3, pp. 338–342, May 1974.
- [51] S. Kimura and W. Butt, “Core-Peripheral Temperature Gradient and Skin Temperature as Predictors of Major Adverse Events Among Postoperative Pediatric Cardiac Patients,” *J. Cardiothorac. Vasc. Anesth.*, pp. S1053-0770(21)00429–8, May 2021, doi: 10.1053/j.jvca.2021.05.018.
- [52] V. Alexi-Meskishvili, S. A. Popov, and A. P. Nikoljuk, “Evaluation of hemodynamics in infants and small babies after open heart surgery,” *Thorac. Cardiovasc. Surg.*, vol. 32, no. 1, pp. 4–9, Feb. 1984, doi: 10.1055/s-2007-1023335.
- [53] D. Cuesta-Frau, M. Varela-Entrecanales, R. Valor-Perez, and B. Vargas, “Development of a novel scheme for long-term body temperature monitoring: a review of benefits and applications,” *J. Med. Syst.*, vol. 39, no. 4, p. 209, Apr. 2015, doi: 10.1007/s10916-015-0209-3.
- [54] B. B. Lahiri, S. Bagavathiappan, T. Jayakumar, and J. Philip, “Medical applications of infrared thermography: A review,” *Infrared Phys. Technol.*, vol. 55, no. 4, pp. 221–235, Jul. 2012, doi: 10.1016/j.infrared.2012.03.007.
- [55] L. J. Jiang *et al.*, “A perspective on medical infrared imaging,” *J. Med. Eng. Technol.*, vol. 29, no. 6, pp. 257–267, Dec. 2005, doi: 10.1080/03091900512331333158.
- [56] B. Kateb, V. Yamamoto, C. Yu, W. Grundfest, and J. P. Gruen, “Infrared thermal imaging: A review of the literature and case report,” *NeuroImage*, vol. 47, pp. T154–T162, Aug. 2009, doi: 10.1016/j.neuroimage.2009.03.043.
- [57] R. B. Knobel, B. D. Guenther, and H. E. Rice, “Thermoregulation and Thermography in Neonatal Physiology and Disease,” *Biol. Res. Nurs.*, vol. 13, no. 3, pp. 274–282, Jul. 2011, doi: 10.1177/1099800411403467.
- [58] E. F. J. Ring and K. Ammer, “Infrared thermal imaging in medicine,” *Physiol. Meas.*, vol. 33, no. 3, pp. R33–46, Mar. 2012, doi: 10.1088/0967-3334/33/3/R33.
- [59] M. Mostafa, N. A. Helmy, A. S. Ibrahim, M. Elsayad, and A. M. Hasanin, “Accuracy of infrared thermography in detecting febrile critically ill patients,” *Anaesth. Crit. Care Pain Med.*, vol. 40, no. 5, p. 100951, Oct. 2021, doi: 10.1016/j.accpm.2021.100951.
- [60] M. Tepper, R. Neeman, Y. Milstein, M. Ben-David, and I. Gannot, “Thermal imaging method for estimating oxygen saturation,” *J. Biomed. Opt.*, vol. 14, no. 5, p. 054048, Sep. 2009, doi: 10.1117/1.3251036.
- [61] R. A. Sherman, A. L. Woerman, and K. W. Karstetter, “Comparative effectiveness of videothermography, contact thermography, and infrared beam thermography for scanning relative skin temperature,” *J. Rehabil. Res. Dev.*, vol. 33, no. 4, pp. 377–386, Oct. 1996.
- [62] J. Kolikof, K. Peterson, and A. M. Baker, “Central Venous Catheter,” in *StatPearls*, Treasure Island (FL): StatPearls Publishing, 2021. Accessed: Jul. 08, 2021. [Online]. Available: <http://www.ncbi.nlm.nih.gov/books/NBK557798/>
- [63] C. Ladakis *et al.*, “Central Venous and Mixed Venous Oxygen Saturation in Critically Ill Patients,” *Respiration*, vol. 68, no. 3, pp. 279–285, 2001, doi: 10.1159/000050511.

- [64] “ICI IR-Pad 640 P-Series IR Camera | Infrared Cameras Inc,” *Infrared Cameras, Inc.*
<https://infraredcameras.com/product/ir-pad-640-medical/> (accessed Jul. 08, 2021).
- [65] “Approaches to Registering Images - MATLAB & Simulink.”
<https://www.mathworks.com/help/images/approaches-to-registering-images.html> (accessed Dec. 01, 2021).
- [66] “Fit geometric transformation to control point pairs - MATLAB fitgeotrans.”
<https://www.mathworks.com/help/images/ref/fitgeotrans.html> (accessed Dec. 01, 2021).
- [67] A. Goshtasby, “Image registration by local approximation methods,” *Image Vis. Comput.*, vol. 6, no. 4, pp. 255–261, Nov. 1988, doi: 10.1016/0262-8856(88)90016-9.
- [68] W. R. Crum, T. Hartkens, and D. L. G. Hill, “Non-rigid image registration: theory and practice,” *Br. J. Radiol.*, vol. 77 Spec No 2, pp. S140-153, 2004, doi: 10.1259/bjr/25329214.
- [69] H. R. Matthews, J. B. Meade, and C. C. Evans, “Peripheral vasoconstriction after open-heart surgery,” *Thorax*, vol. 29, no. 3, pp. 338–342, May 1974.
- [70] B. M. Schey, D. Y. Williams, and T. Bucknall, “Skin temperature as a noninvasive marker of haemodynamic and perfusion status in adult cardiac surgical patients: an observational study,” *Intensive Crit. Care Nurs.*, vol. 25, no. 1, pp. 31–37, Feb. 2009, doi: 10.1016/j.iccn.2008.05.003.

APPENDICES

Appendix A: IRB Approved Clinical Protocol

Thermographic Imaging:

A Novel Method of Diagnostic Hemodynamic Monitoring

Version Date 10/26/2020

A. Project Aim:

The aim of this proposal is to validate thermographic imaging via skin thermography as a surrogate marker of endothelial function and skin microcirculation. Using those data, we further aim to determine if thermographic imaging after corrective or palliative cardiac surgery in patients 5 years of age or less adds additional diagnostic value in predicting impending low cardiac output syndrome as compared to the current standard of care and continuous systemic venous saturation monitoring.

Specific Aim1: Define low cardiac output in subject population, patients 5 years of age or less undergoing corrective or palliative cardiac surgery.

Specific Aim2: Test the null hypothesis that additional information obtained from thermographic imaging adds no additional diagnostic value in predicting low cardiac output syndrome above that of current standard of care.

B. Background:

Advances in surgical technique and improvements in cardiopulmonary bypass (CPB) over the last 20 years have led to significant decreases in CPB related mortality. However, the inflammatory cascade initiated by CPB continues to have a number of well-known deleterious effects on the cardiovascular system leading to diffuse endothelial activation and dysfunction [1]. Infants undergoing corrective or palliative surgery for congenital heart disease are particularly susceptible to these microvascular and endothelial changes manifest by a constellation of clinical signs and symptoms constituting low cardiac output syndrome (LCOS) [2] following their operation. Previous studies suggest that the incidence of LCOS in this population is as high as 24% with an associated mortality rate as high as 20% [3, 4]. LCOS is defined by a decrease in systemic perfusion causing an imbalance of oxygen delivery and consumption at the tissue level

that ultimately leads to metabolic acidosis. LCOS carries high risk for morbidity and mortality without prompt recognition and appropriate intervention [2, 5]. A combination of clinical, hemodynamic, and biochemical parameters is typically used to determine evolving LCOS. Among these indicators are urinary output, heart rate, mixed venous oxygen saturation, central venous pressure, and lactate acid production. In the PRIMACORP Trial, Hoffman et al. specifically defined LCOS as a constellation of the following clinical features: 1) Tachycardia 2) Oliguria, 3) Cold extremities, 4) Cardiac arrest, 5) $\geq 30\%$ difference in arterial and systemic venous saturation (SVO₂) and 6) Metabolic acidosis (increased based deficit >4 or lactate > 2 mg/dl) on 2 successive blood gases [6]. Continuous SVO₂ monitoring has shown promise in predicting outcomes in single ventricle patients after Stage 1 palliation. In an analysis of 116 single ventricle patients who underwent Stage I palliation at their institution from 1996 to 2006, Tweddell et al showed that changes in SVO₂ level in the first six hours after presentation to the intensive care unit was statistically significant in predicting three outcome categories: 1) Survival without complication, 2) survival with complications, and 3) early death. Patients in the latter category had the lowest SVO₂'s in the first six hours. These data demonstrating the utility of SVO₂ monitoring were further supported by the 2012 Surviving Sepsis Campaign which supported early goal directed therapy, particularly targeted SVO₂ goals as a marker of tissue perfusion, to improve the outcome and survival of patients with sepsis. While the utility of continuous SVO₂ monitoring is widely accepted as a reliable marker of tissue oxygenation, doing so requires specialized catheters and monitors making its utility limited on a wide scale do to cost and limited availability. To that end, other measures of tissue perfusion such as near-infrared spectroscopy (NIRS) estimation of tissue oxygenation, continuous clinical capillary refill testing and palpation of skin surface temperature of the extremities have been utilized to make moment to moment assessments. These methods are too not without limitations. NIRS is expensive, subject to inconsistency and provides only highly localized assessment of perfusion. Capillary refill is subjective at best and fraught with inherent operator variability that makes reproducibility of results between individuals virtually impossible.

Systemic vascular resistance and other hemodynamic conditions influence peripheral skin temperature. Such influences at the microvascular level are not considered with simple one-point peripheral temperature measurement. Despite these and other shortcomings, one-point peripheral skin temperature remains one of the cornerstones of bedside assessment as well as basis for changes in treatment in spite of multiple studies that question its utility and accuracy [7-10].

Aside from changes in NIR's and continuous SVO₂ monitoring, all of the other afore described clinical changes are later manifestation of earlier microvascular and endothelial changes leading to LCOS. Consequently, one can easily envision that any new method that provides non-invasive continuous testing of this dysfunction of the vascular endothelium would provide opportunity for detection and intervention before disease is clinically manifested.

The ideal test of perfusion would be non-invasive, inexpensive, reliable, reproducible, and provide no additional risk to the patient. Thermographic imaging provides such promise. In 2014 a case report was published utilizing skin temperature measured by thermographic imaging to detect early stages of shock in a pediatric patient [15]. Thermographic imaging (Fig. 1) is a not new technology, but utilization to determine endothelial function and microvascular perfusion is a novel application. Thermography allows precise multi-point temperature discrimination that is accurate, affordable, portable, and reproducible. It detects infrared radiation emitted from the surface of an object. The emitted infrared radiation is related to the object's temperature by way of cutaneous heat radiation. Every material has an associated emissivity value representing the material's effectiveness in emitting thermal radiation with values ranging from 0 to 1. The closer to 1 an object's emissivity value, the closer and more reliable the temperature measured will be to the actual surface temperature. The emissivity of skin is approximately 0.98 making human skin particularly suitable for temperature measurement using thermography [16]. In fact, noncontact temperature measurement via thermography may be more accurate than contact-based methods [17]. These advantages address many of the current shortcomings of peripheral temperature measurement by touch or a local thermistor and make thermography a novel, non-invasive monitoring modality. Furthermore, the ability of thermographic technology to discriminately measure thousands of temperature points in one image allows for global more physiologically relevant conclusions (i.e., The overall temperature from the hip to the foot is the same; however, there is an area of focal increased temperature over the left knee suggesting a potential inflammatory process.) There is currently extremely limited data available on the vast clinical potentials for this technology. This proposal aims to close that knowledge gap.

C. Preliminary Data:

While thermography has a broad range of applications, reports of clinical utility have been limited. Rich, et al described the use of thermographic imaging to detect pneumothorax in experimental rat models [18]. In 2012, researchers used thermographic imaging to detect minute temperature changes consistent with deposits of brown adipose tissue in healthy children [19]. The documented ability of thermographic imaging to detect early shock in a pediatric patient [15] highlights the vast potential of this novel approach. Extensive work has been done describing baseline thermographic data in upper and lower limbs of healthy adults [16]. These data established several key principles regarding the nature of thermographic images in healthy adult subjects. The first principle is the general symmetry in terms of mean temperatures for both sides of the body as shown in Figure 2. Also observed, the mean temperatures of extremities such as fingers, toes, or dorsal surfaces of the feet are lower in relation to their “core” areas, namely, the volar and plantar surfaces. Finally, when considering the hands, there is a decrease in temperature from the thumb to the fifth digit. In the feet, the hallux and fifth digit have elevated temperatures in relation to the second, third, and fourth digits. Such baseline thermographic data has not yet been generated in the pediatric population.

D. Research Design and Methods:

Specific Aim1

Rationale: Low cardiac output syndrome (LCOS) is a well-recognized entity and has a clear physiological definition, inadequate oxygen delivery to meet tissue metabolic demands. However, there is not a universally accepted clinical definition for LCOS. Continuous superior vena caval oxygen saturation (ScVO₂) monitoring has been widely accepted surrogate marker of oxygen consumption and oxygen delivery at the tissue level. In order to study the performance of thermographic imaging as a reliable surrogate maker of tissue oxygenation and cardiac output, a standard of comparison must be established. Consequently, ScVO₂ in combination with other clinical markers will be used as the “gold standard” by which to test the index marker, thermographic imaging.

Experimental Design: Patients will be consented and enrolled in the study prior to going to the operating room for their corrective or palliative surgery. Typically, a 4 French Cook double lumen central venous catheter is placed in the internal jugular vein preoperatively by cardiac

anesthesia. This catheter is utilized for medication administration, monitoring, transfusion of blood products or intravascular volume expansion as a part of standard post operative care. Instead of the afore mentioned catheters, patients enrolled in the study will have 4.5 French Edward LifeSciences 8 cm Pediasat catheters placed in the super vena caval position by internal jugular approach (performed by cardiac anesthesia) In addition to the normal use of central venous catheters as afore described, these catheters will provide continuous ScVO₂ monitoring during the first 24 hours after surgery. These catheters have been used in previous studies in pediatric patients undergoing cardiac surgery for continuous central venous oxygenation monitoring without catheter related complications (20-22)

Expected Outcome: Continuous ScVO₂ monitoring in addition to other clinical markers will serve as the basis for defining LCOS. Specifically, the following criteria will define the presence of LCOS:

- Presence of metabolic acidosis as defined by increased based deficit >4 or lactate > 2 mg/dl) on 2 successive blood gases

- Plus at least one of the following
 - Oliguria
 - Cold extremities
 - Cardiac arrest
 - >= 30% difference in arterial and systemic venous saturation (may use NIRS as surrogate for systemic venous saturation)

Statistical Consideration: Data obtained from ScVO₂ monitoring and surface temperatures obtained from thermographic imaging will be recorded. As ScVO₂ monitoring will be used as the gold standard by which to compare the index test, thermographic imaging, a Bland-Altman plot will be utilized to determine the agreement between the two modalities. Further, a multivariate regression model to predict low cardiac output will be created using recorded hourly urine output, lactate acid, cerebral Near Infrared Spectroscopy (NIRS), ScVO₂, arterial or venous blood pH and base deficit. A similar regression model will be created using the same parameters except replacing ScVO₂ with data obtained from thermographic imaging. The two models will be compared us the F-test to determine which model provides the best statistical fit for prediction of low cardiac output in patients 5 years of age or less after corrective or palliative cardiac surgery.

Specific Aim2

Rationale: In infants with congenital heart defects undergoing corrective or palliative cardiac surgery, early recognition of adverse alterations in tissue perfusion and cardiac output (LCOS) is key to decreasing postoperative mortality and morbidity. Thus, utilization of monitoring strategies, such as thermographic imaging, that yield real-time accurate and reproducible indices of changes in tissue perfusion will increase safety and improve the care of these patients by adding additional diagnostic data above current standards of care and perhaps even detect relevant subclinical changes allowing for early intervention.

Experimental Design: Subjects 5 years of age or less will undergo the routine postoperative care in the Pediatric Cardiac Critical Care Unit at Vanderbilt Monroe Carell Jr. Children's Hospital. Initial imaging will include the entire uncovered body. Subsequently, a minimum of one arm and one leg will remain exposed and thermographs will be taken every minute for the first 24 hours using a Thermographic Camera set above the patient's bed. This will generate a thermographic movie consisting of 1440 frames. The pictures will consist of non-identifying heat scans and several real optical images (photographs) that will be used to optimize and focus the heat scans. The optical images will be deleted and not retained as a part of the study, unless separate explicit consent to do so is obtained, once the nonidentifying heat scan is optimized and focused. The heat scans are only used to determine skin temperatures. These data will be retrospectively correlated with recorded changes in ScVO₂ lactate, urinary output, cerebral Near Infrared Spectroscopy (NIRS), central venous pressure, and arterial/venous blood gas pH, bicarbonate and base deficit level as documented in the electronic medical record. NIRS will be used as a surrogate marker of systemic venous saturation. Core temperatures will be recorded by rectal or esophageal temperature probes on continuous basis. Patients will be determined to have LCOS (yes or no) based criteria previously outline.

Expected Outcome: A widening temperature differential noted on proximal to distal thermographs will correlate to subclinical adverse changes in tissue perfusion and will predict an increase in lactate acid production, decrease in urinary output, decrease in NIRs, increase in central venous pressure, and evolution of a metabolic acidosis as measured by a concurrent decrease in pH and bicarbonate level along with an increasing base deficit.

Statistical Consideration: Using normative data obtained per Specific Aim1, a linear model (slope intercept form) of the observed temperature differential of the measured body surface (i.e. leg: thigh to toe; arm: shoulder to fingertip) will be created (presuming that the data follows a

linear pattern otherwise non-linear regression modeling will be used). The slope of the model will represent the normal variation in temperature across and extremity from central to peripheral. A similar model (slope intercept form) will be created using data collected via thermography from observed post operative subjects. Perfusion and cardiac output will be deemed normal as the slope of the temperature differential across the extremity of the post operative subject mirrors that from similarly age matched normal controls. Conversely, perfusion and cardiac output will be deemed impaired (i.e LCOS) as the slope of the temperature differential across the extremity of the post operative subject increases above that from similarly age matched normal controls. Subsequently, a logistic regression model will be created to determine how well changes in the temperature differential slope predict deterioration in perfusion and cardiac output (i.e.. LCOS) when compared to current clinical standards.

E. Significance and Future Directions:

As surgical techniques advance and the ability to intervene on patients with congenital heart disease continues to improve, there is shifting focus on the ability of specialized pediatric cardiac intensive care units to support and treat these patients during their period of highest vulnerability, the first 24-hours after operative correction or palliation of their cardiac anomaly. Modalities that increase the provider's awareness of subtle but often ominous changes ultimately lead to earlier therapeutic interventions significantly decreasing morbidity and mortality in this vulnerable patient population. If the proposed hypotheses are proven correct, this research will mark not only a key advance in pediatric cardiac intensive care but also establish the relevance of a key technology that to date has been grossly underutilized in the pediatric population.

F. Investigative Team and Environment:

The principal investigator, Dr. Isaura Diaz, MD, is an American Board of Pediatrics certified Pediatrician and Pediatric Intensive Care physician. She completed residency training at Texas Children's Hospital and her fellowship training at Vanderbilt Monroe Carell Jr. Children's Hospital. She completed advance training in Pediatric Cardiac Intensive Care at Texas Children's Hospital. She has particular interest and expertise in the care of children with heart failure and the additional support of those children with mechanical ventricular assist devices. Dr. Diaz has formulated an expert research team that will ensure the success of this project. She has collaborated with Justin Baba, Ph.D., who has expertise in Biomedical Engineering. Dr. Baba has technical expertise in thermographic imaging and measurement. Further partnership with the

Division of Pediatric Cardiothoracic Surgery will ensure the seamless enrollment of patients who meet inclusion criteria and consent to the study

The Monroe Carell, Jr. Children's Hospital at Vanderbilt is a 277-bed free-standing facility built in 2004, which opened a \$30 million 30,000 sq. ft. expansion in May of 2012. In 2012, Children's Hospital was recognized as one of the top children's hospitals in the nation by U.S. News & World Report, ranking in all 10-specialty areas including heart surgery. The Division of Pediatric Cardiac Surgery has 3 full time faculty performing between 450 to 500 pediatric cardiac surgery cases per year.

Clinical Protocol References:

1. Beghetti, M., et al., Decreased exhaled nitric oxide may be a marker of cardiopulmonary bypass induced injury. *Ann Thorac Surg*, 1998. 66(2): p. 532-4.
2. Hoffman, T.M., et al., Efficacy and safety of milrinone in preventing low cardiac output syndrome in infants and children after corrective surgery for congenital heart disease. *Circulation*, 2003. 107(7): p. 996-1002.
3. Parr, G.V., E.H. Blackstone, and J.W. Kirklin, Cardiac performance and mortality early after intracardiac surgery in infants and young children. *Circulation*, 1975. 51(5): p. 867-74.
4. Wernovsky, G., et al., Postoperative course and hemodynamic profile after the arterial switch operation in neonates and infants. A comparison of low-flow cardiopulmonary bypass and circulatory arrest. *Circulation*, 1995. 92(8): p. 2226-35.
5. Wessel, D.L., Managing low cardiac output syndrome after congenital heart surgery. *Crit Care Med*, 2001. 29(10 Suppl): p. S220-30.
6. Hoffman, T.M., et al., Prophylactic intravenous use of milrinone after cardiac operation in pediatrics (PRIMACORP) study. *Prophylactic Intravenous Use of Milrinone After Cardiac Operation in Pediatrics*. *Am Heart J*, 2002. 143(1): p. 15-21.
7. Murdoch, I.A., et al., Core-peripheral temperature gradient in children: does it reflect clinically important changes in circulatory haemodynamics? *Acta Paediatr*, 1993. 82(9): p. 773-6.
8. Ross, B.A., L. Brock, and A. Aynsley-Green, Observations on central and peripheral temperatures in the understanding and management of shock. *Br J Surg*, 1969. 56(12): p. 877- 82.
9. Ryan, C.A. and C.M. Soder, Relationship between core/peripheral temperature gradient and central hemodynamics in children after open heart surgery. *Crit Care Med*, 1989. 17(7): p. 638-40.
10. Vincent, J.L., J.J. Moraine, and P. van der Linden, Toe temperature versus transcutaneous oxygen tension monitoring during acute circulatory failure. *Intensive Care Med*, 1988. 14(1): p. 64-8.

11. Hansell, J., et al., Non-invasive assessment of endothelial function - relation between vasodilatory responses in skin microcirculation and brachial artery. *Clin Physiol Funct Imaging*, 2004. 24(6): p. 317-22.
12. Anderson, T.J., et al., Close relation of endothelial function in the human coronary and peripheral circulations. *J Am Coll Cardiol*, 1995. 26(5): p. 1235-41.
13. Lieberman, E.H., et al., Flow-induced vasodilation of the human brachial artery is impaired in patients <40 years of age with coronary artery disease. *Am J Cardiol*, 1996. 78(11): p. 1210-4.
14. Takase, B., et al., Endothelium-dependent flow-mediated vasodilation in coronary and brachial arteries in suspected coronary artery disease. *Am J Cardiol*, 1998. 82(12): p. 1535-9, A7-8.
15. Ortiz-Dosal, G., Rina Rus, Anja Koren-Jeverica, Tadej Avcin, Rafael Ponikvar, Jadranka Buturovic-Ponikvar, Use of Infrared Thermography in Children with Shock: A Case Series *SAGE Open Medical Case Reports*, 2014. 2: p. 1-5
16. Gatt, A., et al., Thermographic patterns of the upper and lower limbs: baseline data. *Int J Vasc Med*, 2015. 2015: p. 831369.
17. Sherman, R.A., A.L. Woerman, and K.W. Karstetter, Comparative effectiveness of videothermography, contact thermography, and infrared beam thermography for scanning relative skin temperature. *J Rehabil Res Dev*, 1996. 33(4): p. 377-86.
18. Rich, P.B., et al., Infrared thermography: a rapid, portable, and accurate technique to detect experimental pneumothorax. *J Surg Res*, 2004. 120(2): p. 163-70.
19. Symonds, M.E., et al., Thermal imaging to assess age-related changes of skin temperature within the supraclavicular region co-locating with brown adipose tissue in healthy children. *J Pediatr*, 2012. 161(5): p. 892-8.
20. Spenceley, N., et al. Continuous central venous saturation monitoring in pediatrics: a case report. *Pediatr Crit Care Med* 2008, Vol. 9, No. 2, pe13-e16
21. Liakopoulus, O., et al. An Experimental and Clinical Evaluation of a Novel Central Venous Catheter with Integrated Oximetry for Pediatric Patients Undergoing Cardiac Surgery. *Pediatric Anesthesiology*. December 2007 – Volume 105 – Issue 6 – p 1598-1604. doi: 10.1213/01.ane.0000287657.08434.dc
22. Kakuta, N, Kawahito, S, Mita N, et al. Usefulness of central venous oxygen saturation monitoring during bidirectional Glenn shunt. *J Med Invest*. 2013;60(3-4):272-275.doi:10.2152/jmi.60.272

Appendix B: ICI Camera Technical Specifications

Revision: 4.2021-001

ICI | INFRARED CAMERAS INC

IR-PAD 640 P SERIES IR CAMERA



The ICI P Series IR Camera is a winning combination of high pixel resolution and radiometry. It is perfect for indoor use and is a superior thermal imaging product for outdoor work environments. The ultra rugged imager uses our custom ICI P Series IR Camera device to capture your thermal 640 x 512 images and stores them on a 128GB Hard Drive. The unbeatable design is capable of meeting any non-contact thermography needs you may encounter in the field of health services. Includes our IR Flash Software version 1.0.

Specifications

- **Detector Array:** UFPA (VOx)
- **Pixel Pitch:** 17 μ m
- **FOV:** lens dependent
- **Measurement Distance:** lens dependent
- **Pixel Resolution:** 640 x 512
- **Spectral Band:** 7 μ m to 14 μ m
- **Thermal Sensitivity (NETD):**
< (30 mK) 0.03 °C at 30 °C (86 °F)
- **Frame Rate:** 30 Hz
- **Dynamic Range:** 14-bit
- **Temperature Range:** 25 °C to 45 °C (77 °F to 113 °F)
- **Operation Range:** 0 °C to 50 °C (32 °F to 122 °F)
- **Storage Range:** -40 °C to 80 °C (-40 °F to 176 °F)
- **Humidity:** 5% to 95% non-condensing
- **Accuracy:** \pm 0.2 °C (0.36 °F)
- **Pixel Operability:** > 99 %
- **Shock/Vibration:** 75 G/2 G
- **Dimensions:**
211 mm x 303 mm x 54 mm (L x W x D \pm 0.5 mm)
(8.31" x 11.93" x 2.13" (L x W x H \pm 0.02"))
- **Power:** 12 V DC 2.58 A, < 36 W
- **Battery:** Lithium battery, built-in, rechargeable
- **Weight (without lens):** 1660 g (3.66 lbs)
- **Interface:** USB 2.0
- **Video:** Radiometric IR and MP4 Visible
- **Video Format:** MP4, 1920 x 1080 @ 30 fps
- **Video Out:** USB-C
- **Image Format:** JPG
- **Image Polarity:** Iron, White Hot, Black Hot, Rainbow, IR11, IR256, Research, Rainbow Percentage
- **Emissivity Correction:** 0.01 to 1.0
- **IP Rating:** IP 54
- Built-in shutter
- **Operating System:** Windows 10
- **Processor:** 10th Gen Intel Core i5
- **Storage:** 128 GB
- **RAM:** 8 GB
- **Screen size:** 12.3"
- **Screen resolution:** 2736 x 1824, 3:2
- **Touch:** multi-touch enabled
- **Visible cameras:** rear facing 8 MP at 3264 x 2448, front facing 5 MP at 2560 x 1920
- Wi-Fi 802.11ax/ac/n/g/b/a
- Bluetooth® Wireless 5.0
- Stereo microphone and stereo speakers w/ Dolby™ Audio
- Ambient light sensor
- Accelerometer, Gyroscope, and Magnetometer

Features

- IR Camera + tablet system
- Unparalleled image resolution
- Widescreen viewing
- Heavy duty tablet case
- Bluetooth connectivity
- Indoor/outdoor use
- Adjustable neckstrap and stand
- IR Flash version 1.0 Software
- 8 Palettes including B&W

Applications

- Skin temperature measurement
- Hospital healthcare procedures
- Healthcare robotics
- Radiometric imaging
- Scientific research
- Breast imaging
- Airport screening
- Sub-acute healthcare settings

Options/Lenses

- Optional: 1/4"-20 tripod
- Optional: Touch Pen
- Temperature reference source
- 12.5 mm Manual focus lens (50° x 37.5° FOV, +64 g (+2.26 oz))
- 25 mm Athermalized focus lens (24.8° x 18.6° FOV, +50 g (+1.76 oz))
- Integrated visible camera

THIS DEVICE IS INTENDED FOR ADJUNCTIVE USE WITH OTHER CLINICAL DIAGNOSTIC PROCEDURES TO MEASURE HUMAN BODY TEMPERATURE VIA NON-CONTACT SKIN MEASUREMENTS VISUALIZED FROM THE HUMAN FACE. NOT MEANT FOR STANDALONE CLINICAL DIAGNOSTIC PROCEDURES OR TO TREAT OR DIAGNOSE PATIENTS.

ICI cameras fall under US Federal Law and Export Control.

Specifications subject to change without notice.

2105 W. Cardinal Dr. Beaumont, TX 77705 | Phone: (409) 861-0788 | Toll Free: (866) 861-0788
infraredcameras.com | sales@infraredcameras.com | We Are IR™

Appendix C: Clinical Nurse Protocol

Thermographic Imaging Study

(Drs. Baba, Clay, Diaz, Zaki)




- The goal of this study is to detect low cardiac output syndrome in infants using a thermal imaging camera during the first 24 hours after cardiac surgery.
- Ideally, patients should be uncovered. If this is not possible, please leave some of the core and an extremity exposed.
- Please also position the ventilator tubing as much toward the patient's head as possible (ie, tubing not overlying the chest)
- There may also be an additional monitor in the room (Edwards LifeSciences EV1000). In order to keep the study blinded, please keep the screen covered at all times.

If you have any questions, please contact any of the investigators above. You may also reach Dr. Zaki at (757) 536-6345.

Thermographic Imaging Study

(Drs. Baba, Clay, Diaz, Zaki)

- The goal of this study is to detect low cardiac output syndrome in infants using a thermal imaging camera during the first 24 hours after cardiac surgery.

<ul style="list-style-type: none"> • Ideally, patient should be supine and uncovered. • If this is not possible, please leave some of the core and extremity exposed. 	<p style="text-align: center;">GOOD</p> 	<p style="text-align: center;">BAD</p> 
<ul style="list-style-type: none"> • Please also position the ventilator tubing towards the patient's head as much as possible (ie, tubing not overlying the chest) • There may also be an additional monitor in the room (Edwards LifeSciences EV1000). In order to keep the study blinded, please keep the screen covered at all times. 		<p>To the left is a good example of a swaddled patient</p> <p>Core and leg exposed Tubes situated to the side of head</p>